Die approbierte gedruckte Originalversion dieser Diplomarbeit ist an der TU Wien Bibliothek verfügbar
The approved original version of this thesis is available in print at TU Wien Bibliothek.

Diplomarbeit

Quantum Foundation Experiments with Active Feed-Forward

zur Erlangung des akademischen Grades

Diplom-Ingenieur

im Rahmen des Studiums

Technischer Physik

eingereicht von

Michael Antesberger

Matrikelnummer: 01425873

Ausgeführt am
[1]Atominstitut der Technischen Universität Wien
in Zusammenarbeit mit dem Institut für
[2]Quantenoptik, Quantennanophysik und Quanteninformation der Universität Wien

Unter Betreuung von
Dr. Lee Rozema[2]
Univ. Prof. Dipl. Ing. Dr. Philip Walther[2]
Univ. Prof. Dipl.-Phys. Dr.rer.nat. Thorsten Schumm[1]

Ort, Datum	Michael Antesberger	Thorsten Schumm

Die approbierte gedruckte Originalversion dieser Diplomarbeit ist an der TU Wien Bibliothek verfügbar
The approved original version of this thesis is available in print at TU Wien Bibliothek.

Die approbierte gedruckte Originalversion dieser Diplomarbeit ist an der TU Wien Bibliothek verfügbar
The approved original version of this thesis is available in print at TU Wien Bibliothek.

TECHNISCHE UNIVERSITÄT WIEN
Vienna University of Technology

Master thesis

Quantum Foundation Experiments with Active Feed-Forward

Submitted in partial fulfillment of the requirements for the degree of

Diplom-Ingenieur

in

Technical Physics

submitted by

Michael Antesberger

Student number: 01425873

Executed at the
[1]Atominstitut of the Vienna University of Technology
in collaboration with the institute for
[2]Quantum Optics, Quantum Nanophysics and Quantum Information of the University of Vienna

Under the guidance of
Dr. Lee Rozema[2]
Univ. Prof. Dipl. Ing. Dr. Philip Walther[2]
Univ. Prof. Dipl.-Phys. Dr.rer.nat. Thorsten Schumm[1]

Place, Date	Michael Antesberger	Thorsten Schumm

Die approbierte gedruckte Originalversion dieser Diplomarbeit ist an der TU Wien Bibliothek verfügbar
The approved original version of this thesis is available in print at TU Wien Bibliothek.

Erklärung zur Verfassung der Arbeit

Michael Antesberger, BSc

Hiermit erkläre ich, dass ich diese Arbeit selbständig verfasst habe, dass ich die verwendeten Quellen und Hilfsmittel vollständig angegeben habe und dass ich die Stellen der Arbeit – einschließlich Tabellen, Karten und Abbildungen –, die anderen Werken oder dem Internet im Wortlaut oder dem Sinn nach entnommen sind, auf jeden Fall unter Angabe der Quelle als Entlehnung kenntlich gemacht habe.

Ort, Datum	Michael Antesberger

Die approbierte gedruckte Originalversion dieser Diplomarbeit ist an der TU Wien Bibliothek verfügbar
The approved original version of this thesis is available in print at TU Wien Bibliothek.
TU WIEN Bibliothek Your knowledge hub

Die approbierte gedruckte Originalversion dieser Diplomarbeit ist an der TU Wien Bibliothek verfügbar
The approved original version of this thesis is available in print at TU Wien Bibliothek.

Abstract

This work consists of two different experiments from the field of quantum foundations and quantum information. Both are based on an active feed-forward protocol [1], with which the path of individual photons in the experimental setup can be controlled. Since these two experiments were performed independently, both are briefly summarized in separate paragraphs.

Maxwell's demon is a thought experiment from 1867 in which a demon can lower the total entropy of two initially equalised thermal baths, without performing any work on the system [2]. The discussions that arose initially due to the apparent violation of the second law of thermodynamics have continued to this day. One of the reasons for this is that the thought experiment provides a direct link between quantum information processing and thermodynamics. In this work, we transferred the thought experiment into a photonic domain based on fiber optic components. Therefore, we use thermal states of light in place of thermal baths. This gives us access to new tools, like ultra fast optical switches and the ability to create more interesting states. Moreover, we have verified experimentally, that certain correlations between the thermal baths can tremendously enhance the 'power' of Maxwell's demon, while others eliminate his influence completely.

The field of indefinite causal order in quantum mechanics has seen more and more interest in the past years, both theoretically [3] and experimentally [4]. In such processes, different parties act in a superposition of different orders. Since the first experimental realization of a process with an indefinite causal order, the quantum SWITCH, several protocols taking advantage of this new resource have emerged. In previous experiments, the causal non-separability of two parties has been verified by measuring a so-called 'causal witness' [5]. Nevertheless, the corresponding process matrix has only been evaluated theoretically. Here, we experimentally reconstruct the process matrix of a new passively-stable fiber-based architecture for the quantum SWITCH based on time-bin encoded qubits, which can readily be

Die approbierte gedruckte Originalversion dieser Diplomarbeit ist an der TU Wien Bibliothek verfügbar
The approved original version of this thesis is available in print at TU Wien Bibliothek.
TU Bibliothek Your knowledge hub WIEN

scaled to more parties. We perform a full characterization of this new type of quantum SWITCH by implementing causal process tomography for the first time. We then compare the tomography results to those obtained by directly measuring several different causal witnesses. Finally, we present the first measurement of the fidelity of our experimental quantum SWITCH to the ideal quantum SWITCH.

Die approbierte gedruckte Originalversion dieser Diplomarbeit ist an der TU Wien Bibliothek verfügbar
The approved original version of this thesis is available in print at TU Wien Bibliothek.
TU Bibliothek Your knowledge hub WIEN

Kurzfassung

Diese Arbeit besteht aus zwei verschiedenen Experimenten aus dem Gebiet 'quantum foundations' und Quanteninformation. Beide basieren auf einem aktiven Feedforward-Protokoll [1], mit dem der Pfad einzelner Photonen im Versuchsaufbau beeinflusst werden kann. Da diese beiden Experimente unabhängig voneinander durchgeführt wurden, werden beide in separaten Absätzen kurz zusammengefasst.

Der Maxwell-Dämon ist ein Gedankenexperiment aus dem Jahr 1867, bei dem ein Dämon die Gesamtentropie von zwei zunächst sich im Gleichgewicht befindlichen Behälter, gefüllt mit Luftmolekülen senken kann. Dabei verrichtet er keine Arbeit am System Arbeit [2]. Die Diskussionen, die zunächst aufgrund der scheinbaren Verletzung des zweiten Hauptsatzes der Thermodynamik entstanden sind, haben sich bis heute fortgesetzt. Einer der Gründe dafür ist, dass das Gedankenexperiment eine direkte Verbindung zwischen Quanteninformationsverarbeitung und Thermodynamik darstellt. In dieser Arbeit transferierten wir das Gedankenexperiment in eine photonische Plattform basierend auf faseroptischen Komponenten. Daher verwenden wir thermische Lichtzustände anstelle von mit Luftmolekülen gefüllte Behälter. Dies gibt uns Zugang zu neuen Werkzeugen, wie z.B. ultraschnelle optische Schalter, so wie die Möglichkeit interessantere Zustände zu erzeugen. Darüber hinaus haben wir experimentell nachgewiesen, dass bestimmte Korrelationen zwischen den Thermalbädern die 'Wirksamkeit' des Maxwellschen Dämons enorm steigern können, während andere seinen Einfluss vollständig eliminieren.

Das Gebiet der unbestimmten kausalen Ordnung in der Quantenmechanik hat in den letzten Jahren sowohl theoretisch [3] als auch experimentell [4] immer mehr Aufmerksamkeit erhalten. In solchen Prozessen agieren verschiedene Parteien in einer Superposition von unterschiedlichen kausalen Abfolgen. Seit der ersten experimentellen Realisierung eines Prozesses mit unbestimmter kausaler Abfolge, dem Quanten-SWITCH, sind mehrere Pro-

Die approbierte gedruckte Originalversion dieser Diplomarbeit ist an der TU Wien Bibliothek verfügbar
The approved original version of this thesis is available in print at TU Wien Bibliothek.
TU WIEN Bibliothek Your knowledge hub

tokolle entstanden, die diese neue Ressource nutzen. In früheren Experimenten wurde die kausale nicht-Separierbarkeit zweier Ereignisse durch die Messung eines sogenannten 'kausalen Zeugen' überprüft [5]. Dennoch wurde die entsprechende Prozessmatrix nur theoretisch evaluiert. In dieser Arbeit rekonstruieren wir experimentell die Prozessmatrix einer neuen passiv-stabilen faserbasierten Architektur für den Quanten-SWITCH, welcher auf Time-Bin kodierten Qubits basiert. Dieses Konzept kann leicht auf eine mehr-Parteien-Variante erweitert werden. Wir führen eine vollständige Charakterisierung dieses neuen Typs des Quanten-SWITCH durch, indem wir erstmals Quantenprozesstomographie auf diesem durchführen. Anschließend vergleichen wir die Ergebnisse der Tomographie mit denen, die wir durch die Messungen verschiedener 'kausalen Zeugen' erhalten haben. Zum Schluss präsentieren wir die erste Messung der Fidelität unseres experimentellen Quanten-SWITCH zum idealen Quanten-SWITCH.

Die approbierte gedruckte Originalversion dieser Diplomarbeit ist an der TU Wien Bibliothek verfügbar
The approved original version of this thesis is available in print at TU Wien Bibliothek.
TU Bibliothek Your knowledge hub WIEN

Contents

Abstract **iii**

Kurzfassung **v**

1 Introduction **1**
1.1 Enhanced Photonic Maxwell's Demon with correlated Baths . 1
1.2 Quantum Switch with Time-Bin encoded Qubits 2

2 Theory **3**
2.1 Active Feed-Forward 3
2.2 Photon Sources 4
2.2.1 Second Order Correlation Function 4
2.2.2 Thermal Light Source 5
2.2.3 Spontaneous Parametric Down Conversion 6
2.2.4 NOON-State Generation 7
2.3 Photonic Maxwell's Demon 8
2.3.1 Maxwell's Demon - A Thought Experiment 8
2.3.2 Principle of the Photonic Maxwell's Demon 9
2.4 Quantum Switch with Time-Bin encoded Qubits 20
2.4.1 The n-SWITCH Operation 21
2.4.2 Qubit Encoding 23
2.4.3 Polarization single-Qubit Gates 24
2.4.4 The Causal Witness 26
2.4.5 Quantum Process Tomography 29

3 Experimental Setup **33**
3.1 Photonic Maxwell's Demon 33
3.2 Quantum SWITCH 35

4 Results **41**
4.1 Photonic Maxwell's Demon 41
4.1.1 Characterization of the Photon States 41
4.1.2 The 'Power' of the photonic Maxwell's Demon 42

Die approbierte gedruckte Originalversion dieser Diplomarbeit ist an der TU Wien Bibliothek verfügbar
The approved original version of this thesis is available in print at TU Wien Bibliothek.
TU WIEN Bibliothek Your knowledge hub

4.2 Quantum SWITCH 45
4.2.1 The 2-SWITCH Operation with Pauli-Operators 45
4.2.2 Witnessing Causal Non-Separability 47
4.2.3 Process Tomography 52

5 Conclusion & Outlook **55**
5.1 Photonic Maxwell's Demon 55
5.2 Fiber-Based Quantum SWITCH 55

Appendices **57**

A Fiber Polarization Compensation **59**

Acknowledgments **61**

Die approbierte gedruckte Originalversion dieser Diplomarbeit ist an der TU Wien Bibliothek verfügbar
The approved original version of this thesis is available in print at TU Wien Bibliothek.
TU Bibliothek Your knowledge hub WIEN

Die approbierte gedruckte Originalversion dieser Diplomarbeit ist an der TU Wien Bibliothek verfügbar
The approved original version of this thesis is available in print at TU Wien Bibliothek.
TU WIEN Bibliothek Your knowledge hub

Chapter 1

Introduction

1.1 Enhanced Photonic Maxwell's Demon with correlated Baths

While the development of Maxwell's theory of heat [2] in the 19th century, he proposed a thought experiment in 1867, which became known as Maxwell's Demon. In this proposal, there is supernatural creature, a demon, who can lower the total entropy of two baths, which were initially in thermal equilibrium, without applying any work. This statement has sparked innumerable debates as it would violate the second law of thermodynamics. This violation was settled by Landauer's introduction of the information entropy [6]. He claimed that, eventually the demon has to run out of memory for storing the information acquired from the particles. Hence, he has to start erasing information. Since erasing information is a thermodynamic irreversible process, this results in an increase of entropy. Nevertheless, the discussions around the thought experiment have continued, since it represents a relation between thermodynamics and information theory.

Recently, Vidrighin *et al* [7] implemented a proof of principle experiment, showing that Maxwell's demon can be transferred to the photonic domain by realizing the thermal baths as photonic spatial modes of pseudo thermal light. Shortly thereafter, Shu *et al* presented a theoretical proposal showing that the effect of the demon, the demon's 'power', can be greatly enhanced by using states with different correlations between the baths. Hence, we took it as our task to realize the first photonic Maxwell's demon with correlated baths to experimentally verify the theoretical proposal from [8]. In our experiment the demon has the ability of actually swapping particles between baths (optical modes) by implementing a detection dependent active feed-forward protocol.

1.2 Quantum Switch with Time-Bin encoded Qubits

It seems to be quite fundamental that nature is based on phenomena with a fixed causal order. This means that, given two events A and B. A must happen before or after B. For classical physics this also is the case. Not so long ago, however, it was recognized that quantum mechanics also allows processes with an undefined causal order [9][3]. In these processes, it is impossible to say which event accrued first. Such processes are called causally non-separable. The first experimental implementation of such a process, the quantum SWITCH, appeared shortly after and was realized by Procopio *et al* [4]. Moreover, it turned out that this new device also possesses a computational advantage in its query complexity (i.e. how often a quantum gate is called) compared to conventional quantum circuits. However, this property only becomes useful when the number of gates involved is increased. It is not straight forward to implement the architecture from [4] with more then two quantum gates. Nevertheless, interest in the quantum SWITCH has remained both experimentally and theoretically. Following the first demonstration, the causally non-separable order of the quantum gates was experimentally verified by measuring a 'causal witness' on the device.

Although the quantum switch has been the subject of intense research, the mathematical object of the process matrix, which describes the dynamics of a process and thus its causal relations, remained only theoretical. In this work we propose a new passively-stable fiber-based architecture for the quantum SWITCH, which is based on time-bin encoded qubits. We would also like to note that the architecture proposed here can be scaled up to more than two parties. In order to verify the causally non-separable nature of the device, we measured a 'causal witness' and more than that, we experimentally determined for the first time the process matrix of the SWITCH and estimated the fidelity to the ideal object as $F = 0.753$.

Die approbierte gedruckte Originalversion dieser Diplomarbeit ist an der TU Wien Bibliothek verfügbar
The approved original version of this thesis is available in print at TU Wien Bibliothek.
TU Bibliothek Your knowledge hub WIEN

Die approbierte gedruckte Originalversion dieser Diplomarbeit ist an der TU Wien Bibliothek verfügbar
The approved original version of this thesis is available in print at TU Wien Bibliothek.

Chapter 2

Theory

2.1 Active Feed-Forward

Having control over the path taken by single photons in photonic quantum experiments is of general interest in the fields of quantum communication and quantum computation. [10] One way to obtain this control is to perform measurement based feed-forward. In both experiments of this work, we use a new technique developed for fiber-based setups, which was first introduced in [1]. Fig. 2.1 shows the simplest configuration of this procedure.

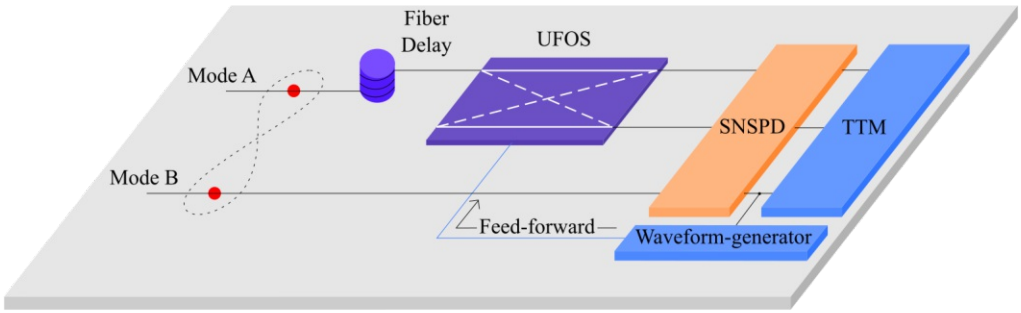

Figure 2.1: This figure illustrates the active feed-forward protocol, which was implemented in both experiments of this work. The infinity-shaped dotted line around the two red photons in mode A and B symbolizes the temporal correlations between both particles. The acronyms used in the figure labels are the same as defined in the text.

Here we have two correlated photons in different spatial modes A and B, the origin of which in our case is either a spontaneous parametric down-conversion photon pair source [11] or thermal light split on a beam splitter [12] The photon in mode B is used for heralding and gets detected by superconducting nanowire single photon detector (SNSPD) from PhotonSpot Inc. (deadtime 50 ns, average system detection efficiency 90%) The detection event is recorded by a commercial time tagging module (UQDevices Logic16; TTM) and triggers a waveform generator (Keysight 33500B Series), which

can output a TTL pulse of arbitrary length. The key component for the feed-forward procedure is a 2x2 ultra fast optical switch (UFOS) from Boston Applied Technologies, Inc. (BATi 2x2 Nanona fiber switch, response time below 60 ns, maximal duty-cycle of 1 MHz, cross-channel isolation greater than 20 dB). The ground state of the optical switch is the cross state, where light in mode A is routed to mode B and vice versa. As the UFOS receives a TTL pulse, it changes its state to bar, where light in mode A is transmitted to mode A and the same for B. Hence, we are able to decide which path the photon in mode A should take. Note, while the heralding signal is being processed, the heralded photon has to be delayed by at least the processing time and the state preparation time of the UFOS, which is approximately 320 ns.

2.2 Photon Sources

In this chapter, the different photon sources, which were used for the experiments and their underlying principles are explained.

2.2.1 Second Order Correlation Function

In the field of quantum optics the second order correlation function is broadly used to distinguish the statistical properties of light fields. Moreover, it is convenient to consider the normalized second order correlation function, which is also referred as degree of second order coherence. It describes the correlation between the intensities of two light fields and can be written as

$$g^{(2)}(\boldsymbol{r}_1, t; \boldsymbol{r}_2, t+\tau) = \frac{\langle \boldsymbol{E}^*(\boldsymbol{r}_1, t)\boldsymbol{E}^*(\boldsymbol{r}_2, t+\tau)\boldsymbol{E}(\boldsymbol{r}_2, t+\tau)\boldsymbol{E}(\boldsymbol{r}_1, t)\rangle}{\langle \boldsymbol{E}^*(\boldsymbol{r}_1, t)\boldsymbol{E}^*(\boldsymbol{r}_1, t)\rangle\langle \boldsymbol{E}^*(\boldsymbol{r}_2, t+\tau)\boldsymbol{E}(\boldsymbol{r}_2, t+\tau)\rangle}, \quad (2.1)$$

where $\boldsymbol{E}$ is the electric field of the light at the position $\boldsymbol{r}_1$, $\boldsymbol{r}_2$ at times t and $t+\tau$ respectively. [17] For the case of stationary fields Eq. 2.1 becomes independent of time t so that $g^{(2)}$ only depends on the time difference τ. Moreover, the correlation function is even, $g^{(2)}(\tau) = g^{(2)}(-\tau)$. For classical fields the Cauchy-Schwartz inequality controls the allowed values of $g^{(2)}(\tau)$ and restricts them to $1 \leq g^{(2)}(0) \leq \infty$. While for τ much bigger than the coherence time τ_c of the light fields $g^{(2)}(\tau) \to 1$ for $\tau \gg \tau_c$ [17].

To transfer Eq. 2.1 to the quantum picture, we replace the electric field vectors their quantum field operators:

$$\boldsymbol{E}^* \to \hat{\boldsymbol{E}}^- \propto \hat{a}^\dagger, \quad (2.2a)$$

$$\boldsymbol{E} \to \hat{\boldsymbol{E}}^+ \propto \hat{a}, \quad (2.2b)$$

Die approbierte gedruckte Originalversion dieser Diplomarbeit ist an der TU Wien Bibliothek verfügbar
The approved original version of this thesis is available in print at TU Wien Bibliothek.
TU Bibliothek Your knowledge hub WIEN

where $\hat{a}$ ($\hat{a}^\dagger$) is the photon annihilation (creation) operator. [17] By splitting an incident photon beam on a symmetric beam splitter, we can determine the correlation function in terms of a coincidence measurement between the reflected (R) and the transmitted (T) path. R and T refer to the positions $\boldsymbol{r}_1$ and $\boldsymbol{r}_2$ in Eq. 2.1. If we now subdivide τ into discrete time segments $\Delta\tau$ and measure over a total time T_{int}, we can express the second order correlation function in terms of photon detection events as

$$g^{(2)}(\tau) = \frac{N_{RT}(\tau)}{N_R N_T} \frac{T_{int}}{\Delta\tau}, \tag{2.3}$$

where τ is now a multiple of $\Delta\tau$, N_R (N_T) are single photon detection events in the reflected (transmitted) arm of the beam splitter and N_{RT} are the coincidences between the two paths with a difference in their arrival time of τ [19].

As mentioned above, depending on the value of $g^{(2)}$, a statement about the statistical properties of the light can be made. So one can say that if $g^{(2)}(0) > g^{(2)}(\tau)$ it is more likely that photons will appear in groups. This effect is known as photon bunching. Thermal light for example has a $g^{(2)}(0) = 2$ and therefore exhibits bunching behavior. Whereas for coherent light, it is characteristic to have a $g^{(2)}(0) = 1$. Otherwise, if $g^{(2)}(0) < g^{(2)}(\tau)$ it is less likely for the photons to propagate close together. This is also known as antibunching. As already mentioned above, for classical fields the Causchy-Schwartz inequality restricts the allowed values of the correlation function to $1 \leq g^{(2)}(0) \leq \infty$. Therefore, this phenomena is of a purely quantum mechanical nature [17].

2.2.2 Thermal Light Source

As just mentioned in Ch. 2.2.1, it is characteristic for thermal light to exhibit a $g^{(2)}(0) = 2$. Due to the rather short coherence time, typically a few femtoseconds, it is extremely difficult to determine the degree of coherence of natural thermal light [19]. This became significantly easier with the introduction of a pseudothermal light source by Martienssen and Spiller [20], which features a much longer coherence time. However, in this work we follow the protocol proposed by Kuusela [19], which is very closely related to the original proposal.

For generating quasi-monochromatic pseudothermal light, a laser beam is focused with a lens on a rotating ground glass, that contains randomly arranged scattering centers. Different grain sizes lead to arbitrary phase differences between the scattered waves. Due to the rotating motion of the ground glass, the light also shows intensity fluctuations in time and thus

Die approbierte gedruckte Originalversion dieser Diplomarbeit ist an der TU Wien Bibliothek verfügbar
The approved original version of this thesis is available in print at TU Wien Bibliothek.
TU Bibliothek Your knowledge hub WIEN

fulfills the requirements of a thermal light source [20]. The pseudothermal light is then collected by a bare single-mode fiber without any focusing optics, which brings the light source down to the single photon level. The coherence time of the light is variable and depends on the rotation speed of the ground glass. For a Gaussian beam profile whose beam waist lies in the plane of the rotating glass, the coherence time can be calculated as

$$\tau_c = \frac{W_0}{v(1+y^2)^{1/2}}, \tag{2.4}$$

where W_0 is the radius of the waist, v the velocity of the scattering centers and y determines, weather the light is collected in the near- ($y \gg 1$) or in the far field ($y \ll 1$) [19]. In the described proposal, the source is always in the configuration to collect light from the far field. A schematic drawing of the experimental arrangement of the source used for this work is shown in Fig. 3.1 a).

2.2.3 Spontaneous Parametric Down Conversion

Spontaneous parametric down conversion (SPDC) is a non-linear optical process in which a highly energetic pump photon with frequency ω_p gets annihilated and two photons with lower energy are created [21]. Out of convention, these are called signal and idler photon with frequency ω_s and ω_i. Typically three-wave mixing is performed in birefringent crystals where the refractive index depends on the polarization and direction of the light that passes through. In general, the down-conversion efficiency is very low and therefore only a few photons undergo the SPDC process. In order to achieve a down-conversion, the frequency- (Eq. 2.5a) and phase matching conditions (Eq. 2.5b) must be satisfied [21]:

$$\omega_i + \omega_s = \omega_p \tag{2.5a}$$

$$\boldsymbol{k}_i + \boldsymbol{k}_s = \boldsymbol{k}_p\,, \tag{2.5b}$$

where $\boldsymbol{k}_j$ are the wave vectors of the three photons. Since $\hbar\omega$ and $\hbar\boldsymbol{k}$ are the energy and momentum of a photon, these relations can be also interpreted as conservation of energy and momentum. Depending on the polarization of the input photon and the two output photons SPDC is categorized in different kinds. For our experiment, however, we use Type-II down conversion, in which the signal and the idler photon have orthogonal polarizations.

The optimum length L_{opt} of the nonlinear crystal for a given phase mismatch $|\Delta k|$ can be expressed as $L_{\text{opt}} = \frac{\pi}{|\Delta k|}$, where $|\Delta k| = k_p - k_i - k_s$ [22]. It is often impossible to obtain a good enough phase matching to benefit

Die approbierte gedruckte Originalversion dieser Diplomarbeit ist an der TU Wien Bibliothek verfügbar
The approved original version of this thesis is available in print at TU Wien Bibliothek.
TU Bibliothek Your knowledge hub WIEN

actually from the whole interaction length. An elegant solution to this problem is the technique known as quasi-phase matching, in which several pieces of nonlinear crystals are set end to end, each piece being of length $\pi/|\Delta k|$, which is also known as the coherence length, but with signs of the electrical susceptibility coefficient $\chi^{(2)}$ alternating from one piece to the next. Energy will always flow from the pump to signal and idler photon as long as the phase between the two optical waves is less than π, whereas if the relative phase is $\geq \pi$ energy flows back to the pump photon. By changing the sign of the nonlinear susceptibility every coherence length, the phase of the polarization wave is shifted by π, which leads to effectively re-phasing the interaction and to monotonic power flow into the down converted waves [22]. In our case, we take advantage of this technique by using a periodically poled $KTiOPO_4$ (PPKTP) crystal, for which the down converted photon pairs have collinear trajectories arranged along the axis of the pump beam.

2.2.4 NOON-State Generation

A photonic NOON-state is a maximally path entangled many-body state of N photons, which are of the form [23]:

$$|\Psi_{NOON}\rangle = \frac{1}{\sqrt{2}}(|N,0\rangle_{a,b} + e^{i\varphi}\,|0,N\rangle_{a,b}) \tag{2.6}$$

Here, N ist the number of photons involved in the state, 0 refers to the vacuum state and φ is the relative phase. It is characteristic that either all N photons are in mode a and zero in mode b or vice versa. Since it is not straight forward to prepare NOON-states with $N > 2$, we focus on the generation of such a state with $N = 2$. This can be achieved fairly easily using a SPDC photon-pair source and a Hong-Ou-Mandel (HOM) interferometer [12].

When two indistinguishable single-photons in individual signal and idler modes enter simultaneously a 50:50 beam splitter, the photons will always group together in one of the output modes (a or b) of the beam splitter [12]. This phenomena is widely known as the HOM-effect. The output state of such a HOM-interferometer is of the form

$$|\Psi_{HOM}\rangle = \frac{1}{\sqrt{2}}(|2,0\rangle_{a,b} + |0,2\rangle_{a,b}), \tag{2.7}$$

which clearly matches the form of Eq. 2.6 for a NOON-state with $N = 2$. If one would perform a coincidence measurement on modes a and b, the probability of detecting a coincidental event between both modes is zero [12]. Therefore, it is from great importance that the two incident photons are

Die approbierte gedruckte Originalversion dieser Diplomarbeit ist an der TU Wien Bibliothek verfügbar
The approved original version of this thesis is available in print at TU Wien Bibliothek.
TU Bibliothek Your knowledge hub WIEN

indistinguishable in all degrees of freedom. Meaning in polarization, wavelength, spectral profile, spatial mode and of course in their arrival time at the beam splitter. However, in practice the photons might be not perfectly indistinguishable, which leads to a non-ideal interferometric visibility $v^2 < 1$. In Eq. 2.33 (see Ch. 2.3.2) we can see, that this results in the presence of the $|1,1\rangle_{A,B}$ term, which expresses the case when the two photons exit the beamsplitter in different output modes. A schematic drawing of a HOM-interferometer is shown in Fig. 3.1 c).

2.3 Photonic Maxwell's Demon

In this section the concept of the original thought experiment on Maxwell's Demon from 1867 [2], as well as our approach to transfer the experiment to a photonic platform, and the theoretical knowledge necessary to understand the protocol are explained in detail.

2.3.1 Maxwell's Demon - A Thought Experiment

Maxwell's demon was a thought experiment by James Clerk Maxwell that was first initiated in 1867. Since its inception, the experiment has been widely discussed as it would challenge the second law of thermodynamics [2]. Maxwell envisioned two chambers A & B with a common massless aperture that can be opened or closed. Both boxes contain a gas in thermal equilibrium, while a supernatural being, a demon, sits over the chambers and controls the gate. He can sense whether a particle with high or low kinetic energy is approaching the door. By opening the gate in the right moments the demon can separate the hot from the cold particles and hence, the gas is no longer in thermal equilibrium. It seems as this operation reduces the entropy of the gas without performing any work. This stands in contradiction with the second law of thermodynamics. [2] Fig. 2.2 shows this process schematically.

Die approbierte gedruckte Originalversion dieser Diplomarbeit ist an der TU Wien Bibliothek verfügbar
The approved original version of this thesis is available in print at TU Wien Bibliothek.
TU Bibliothek Your knowledge hub WIEN

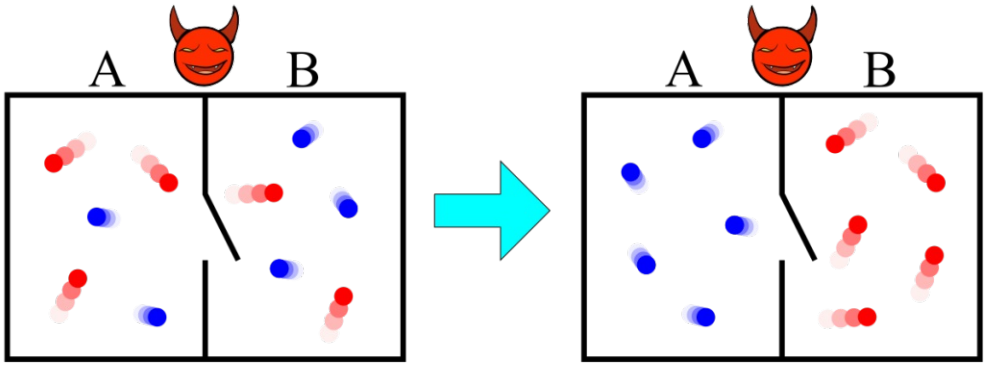

Figure 2.2: This figure illustrates the 'Maxwell's Demon' thought experiment. The left side of the figure, shows two chambers A and B filled with a gas in thermal equilibrium. Blue particles represent lower kinetic energies and hence, a lower temperature. While red indicates the particles have a higher kinetic energy, which corresponds to a higher temperature than the average. Since the demon can sense whether hot or cold particles are approaching the aperture between the chambers, it opens the door to separate hot and cold particles from each other. This leads to a temperature increase in chamber B and a decrease A.

However, Landauer and Bennett argued that the process of erasing information comes hand in hand with an increase in entropy and therefore, the second law of thermodynamics will not be violated. [6][13] More explicitly, to decide weather a particle can pass the door, the demon has to acquire information on the molecule's state. He can store this knowledge, but at some point the demon's storage will be full and he has to erase information again. Erasing information is a thermodynamic irreversible process and therefore increases the entropy. Hence, the total entropy of the system will not be lowered. Since then Maxwell's Demon has remained a widely discussed concept and has seen various experimental demonstrations. [14][15]

2.3.2 Principle of the Photonic Maxwell's Demon

In this work we realize Maxwell's Demon (MD) in a photonic domain. To do so, the thermal baths, represented by the chambers A & B in Fig. 2.2, are implemented as optical modes, each of which hosts a thermal state of photons. Both modes lead to individual SNSPDs, D_A and D_B. The temperatures of the thermal states are directly proportional to the average photon number of each mode. If both detectors register the same number of photons, the baths have the same temperature. Note that, in the experiment, we prepared

Die approbierte gedruckte Originalversion dieser Diplomarbeit ist an der TU Wien Bibliothek verfügbar
The approved original version of this thesis is available in print at TU Wien Bibliothek.
TU Bibliothek Your knowledge hub WIEN

optical thermal states, which contain only a single frequency component and are thus monochromatic. However, such optical states have the same photon statistics as thermal light emitted by a black body in thermal equilibrium and are therefore feasible for realizing thermal baths in an optical domain. The demon can gain information about the photonic state by extracting photons from the individual modes via two variable-reflectivity beam splitters. The reflected outputs are monitored via detectors Dem_A and Dem_B, which are SNSPDs as well. By performing a feed-forward operation (as explained in Ch. 2.1) based on the registered photon detection events, the demon can physically redirect the photons from one mode into the other by controlling an UFOS. Hence, a photonic MD is a device that can create an imbalance in photon number between two modes, which were initially balanced. [16]

A proof of principle of a photonic MD has recently been demonstrated in [7]. In this paper, they implemented a very similar setup to ours, just without an UFOS and detectors D_A and D_B were replaced by conventional photo diodes. The recorded voltage output of the detectors was later fed to a virtual capacitor. They used the information acquired from the reflected ports of the beam splitters and post-processed their data to change the polarity of this virtual capacitor. This induced a non-zero net charge on the capacitor, which allowed them to show the possibility of extracting work from the system. This protocol is more like the post-processing of the photon detection data. In contrast, we can extract work from the photon number imbalance, which is generated by actually sorting the photons of the two optical modes. Since there was a recent theory proposal [8], claiming that correlations between the thermal baths can enhance 'the power of MD', we also want to study this effect on our photonic MD. For that, we measure the photon number difference ΔN between the two modes and quantify 'the power of MD' as the change in photon number per incident photon $\Delta N/N$, where N is the number of detected photons in mode A, which we set always equal to the number of photons in mode B. In the following, we present the derivation of our figure of merit $\Delta N/N$ in the range of low photon numbers for the four different input states used. Fig. 2.3 shows the functional principle of the photonic MD for these different correlated states.

Die approbierte gedruckte Originalversion dieser Diplomarbeit ist an der TU Wien Bibliothek verfügbar
The approved original version of this thesis is available in print at TU Wien Bibliothek.
TU Bibliothek Your knowledge hub WIEN

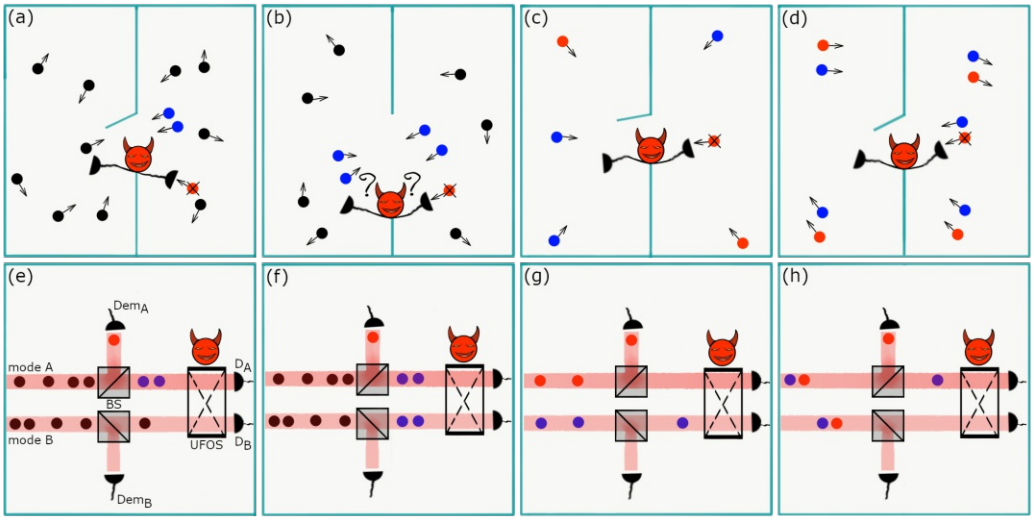

Figure 2.3: This figure illustrates the photon allocation in the presence of a photonic Maxwell's demon. Correlations between photons are indicated by red and blue photons, meaning that, when the demon detects a red photon, he also obtains information about the blue photon. The top row of subfigures represents the particle picture of the photonic MD, while the bottom row shows the implementation via photonic modes. **a)** and **e)**, uncorrelated thermal states: Detecting a photon in Dem_A leads to an increase of photons in mode A. Hence, the two blue particles in mode A. **b)** and **f)**, split thermal states: Since, the modes are correlated, detecting a photon in Dem_A increases the average photon number of both modes. **c)** and **g)**, correlated thermal states: Here, detecting a photon in Dem_A tells the demon that there is another photon in mode B and hence, MD will swap the modes. **d)** and **h)**, anti-correlated thermal states: Since the modes are anti-correlated, a detection event in Dem_A tells the Demon, that there is another photon in mode A and none in mode B. (Figure taken from [16])

Note that the derivations presented below are also given in [16], as this paper was published during this work.

Uncorrelated Thermal States

The density matrix representation is widely used to describe quantum states. The density matrix for a thermal photonic state can be expressed as

$$\rho_{th} = \sum_{n=0}^{\infty} P_n \left|n\right\rangle \left\langle n\right| , \tag{2.8}$$

Die approbierte gedruckte Originalversion dieser Diplomarbeit ist an der TU Wien Bibliothek verfügbar
The approved original version of this thesis is available in print at TU Wien Bibliothek.
TU Bibliothek Your knowledge hub WIEN

where

$$P_n = \frac{\bar{n}^n}{(1+\bar{n})^{n+1}} \qquad \text{and} \qquad \bar{n} = \frac{1}{e^{\beta\hbar\omega} - 1}\,. \tag{2.9}$$

Here P_n is the probability of having n photons in the state, $\bar{n}$ is the average photon number, $\beta = 1/k_b T$ (k_b and T are the Boltzmann constant and the temperature respectively), $\hbar$ is the Planck constant and ω is the angular frequency of the photon. When this state is sent to a beam splitter, the light gets partially reflected into mode Dem_A and transmitted into D_A. The probability to detect m photons in mode D_A and n photons in mode Dem_A is given by

$$P(m,n) = \frac{(m+n)!}{n!m!}\frac{\bar{n}^{n+m}}{(1+n)^{n+m+1}}R^{2n}(1-R^2)^m\,, \tag{2.10}$$

where R is the reflection amplitude of the beam splitter. After the beam splitter, the state can be approximated as

$$\begin{aligned}\rho_{Dem_A,D_A} =& P(0,0)\,|0,0\rangle\,\langle 0,0|_{Dem_A,D_A} + P(1,0)\,|0,1\rangle\,\langle 0,1|_{Dem_A,D_A} + \\ & P(0,1)\,|1,0\rangle\,\langle 1,0|_{Dem_A,D_A} + P(1,1)\,|1,1\rangle\,\langle 1,1|_{Dem_A,D_A} + ...\end{aligned} \tag{2.11}$$

In the derivation of Eq. 2.11 all off-diagonal elements and terms with more than two photons have been ignored. Since we operate in the low photon number regime, hence $P(2,0) \ll P(1,0)$, we have also ignored the terms $P(2,0)\,|0,2\rangle\,\langle 0,2|_{Dem_A,D_A}$ and $P(0,2)\,|2,0\rangle\,\langle 20|_{Dem_A,D_A}$. Since Maxwell's Demon operates with two thermal baths, a state like in Eq. 2.11 is present in modes Dem_A & D_A, and in modes Dem_B & D_B. Therefore, the total input state is $\rho_{Dem_A,D_A} \otimes \rho_{Dem_B,D_B}$ with $\rho_{i,j}$ as in Eq. 2.11.

Now we need to include the demon's process in our calculation. For uncorrelated thermal light, this is illustrated in Fig. 2.3 a), e). If a photon is subtracted from a thermal state (e.g. by means of a beam splitter) the average photon number of the remaining state is doubled ($\bar{n}_{sub} = 2\bar{n}$) [8]. So, if a photon from mode A gets reflected to detector Dem_A, the remaining number of photons in mode A is higher than in mode B. Hence, the two red photons in Fig. 2.3 e). Since the demon wants to increase the photon imbalance between the modes, he will set the UFOS in the 'bar state' and therefore transmits mode A (B) to mode A (B). Note, that we arbitrarily chose to increase the number of photons in mode A. Whereas if a photon gets detected in Dem_B, there are now more photons in mode B than in A, so the demon will set the UFOS to the 'cross state' and route the photons from mode B into mode A. In order to express this process mathematically,

Die approbierte gedruckte Originalversion dieser Diplomarbeit ist an der TU Wien Bibliothek verfügbar
The approved original version of this thesis is available in print at TU Wien Bibliothek.
TU Bibliothek Your knowledge hub WIEN

we make the following substitution:

$$|n,m,0,1\rangle_{A,B,Dem_A,Dem_B} \rightarrow |m,n,0,1\rangle_{A,B,Dem_A,Dem_B} \tag{2.12}$$

Note, that we are not using number resolving detectors and therefore do not swap modes in cases like $|n,m,1,2\rangle$, since we would register a click in both detectors Dem_A and Dem_B. After the demon acts on the thermal states, the output state can be approximated in the low photon number regime as

$$\begin{aligned}\rho_{out} =& P^2(0,0)\,|0000\rangle\langle 0000| + P(0,0)P(0,1)\,|0001\rangle\langle 0001| + \\ & P(0,0)P(1,0)\,|0100\rangle\langle 0100| + P(0,0)P(1,1)\,|1001\rangle\langle 1001| + \\ & P(0,1)P(0,0)\,|0010\rangle\langle 0010| + P^2(0,1)\,|0011\rangle\langle 0011| + \\ & P(0,1)P(1,0)\,|0110\rangle\langle 0110| + P(0,1)P(1,1)\,|0111\rangle\langle 0111| + \\ & P(1,0)P(0,0)\,|1000\rangle\langle 1000| + P(1,0)P(0,1)\,|0101\rangle\langle 0101| + \\ & P^2(1,0)\,|1100\rangle\langle 1100| + P(0,1)P(1,1)\,|1101\rangle\langle 1101| + \\ & P(1,1)P(0,0)\,|1010\rangle\langle 1010| + P(1,1)P(0,1)\,|1011\rangle\langle 1011| + \\ & P(1,1)P(1,0)\,|1110\rangle\langle 1110| + P^2(1,1)\,|1111\rangle\langle 1111| + \dots,\end{aligned} \tag{2.13}$$

where the states are labeled as $|ijkl\rangle_{A,B,Dem_A,Dem_B}$. From Eq. 2.13, we can extract easily the probability for detector D_A or D_B to click:

$$\begin{aligned}P_A =& 2P(0,0)P(1,1) + 2P(1,0)P(1,1) + P(0,0)P(1,0) + \\ & P(0,1)P(1,1) + P^2(1,0) + P^2(1,1)\end{aligned} \tag{2.14a}$$

$$\begin{aligned}P_B =& P(0,0)P(1,0) + 2P(1,0)P(0,1) + 2P(1,0)P(1,1) + \\ & P(0,1)P(1,1) + P^2(1,0) + P^2(1,1)\end{aligned} \tag{2.14b}$$

In our experiment we run this process Γ times and hence measure average single photon rates, which are given by ΓP_A and ΓP_B. Now we can calculate the photon number difference between the modes as $\Delta N = \Gamma(P_A - P_B)$. Inserting Eq. 2.14a and 2.14b results in

$$\begin{aligned}\Delta N =& (2P(0,0)P(1,1) - 2P(0,1)P(1,0))\Gamma \\ & \frac{2\bar{n}^2}{(1-\bar{n})^4}R^2(1-R^2)\Gamma\end{aligned} \tag{2.15}$$

Finally, to derive our figure of merit we divide Eq. 2.15 by the number of input photons N in mode A, which we always set equal to the number of photons in mode B. The probability of having a photon in the input of mode A is $P(1) = \frac{\bar{n}}{(1-\bar{n})}$ and therefore, the input photon rate is given by $N = \Gamma P(1)$. Thus, the demons effect per photon is given by

$$\frac{\Delta N}{N} = \frac{2\bar{n}}{(1-\bar{n})^2}R^2(1-R^2). \tag{2.16}$$

Die approbierte gedruckte Originalversion dieser Diplomarbeit ist an der TU Wien Bibliothek verfügbar
The approved original version of this thesis is available in print at TU Wien Bibliothek.
TU Bibliothek Your knowledge hub WIEN

From Eq. 2.16 we can see that even in the low-photon limit MD's power depends on the average photon number, which is directly related to the temperature of the state. In the following we will show, that this does not apply for correlated and anti-correlated states.

Split Thermal States

Now we want to derive our figure of merit for a split thermal state. To generate such a state, we prepare one thermal state as explained above and send it to a beam splitter. Then we feed the two outputs to the input modes A and B of the demon. Since both input modes originate from the same thermal state, correlations are now present between the modes. If a photon is now subtracted by one of the modes beam splitters, the average photon number is doubled in both modes A & B and hence, the demons effect per photon will be zero. This is illustrated by the two blue photons in each mode in Fig. 2.3 b), f). In the following we will derive this result again mathematically.

For the split thermal state the density matrix can be now written as

$$\rho_{split} = \sum_{n,m=0}^{\infty} P(n,m) \left|n,m\right\rangle \left\langle n,m\right|_{A,B}, \tag{2.17}$$

where $P(n,m)$ is defined as in Eq. 2.10 with $R = 1/\sqrt{2}$. Since we are operating in the low-photon limit, we will again consider only the two photon terms. Moreover, since the output modes of the beamsplitter are not interfered, we can also neglect all off-diagonal elements:

$$\begin{aligned}\rho_{split} \approx & P(0,0) \left|0,0\right\rangle \left\langle 0,0\right|_{A,B} \\ & P(0,1) \left|0,1\right\rangle \left\langle 0,1\right|_{A,B} + P(1,0) \left|1,0\right\rangle \left\langle 1,0\right|_{A,B} \\ & P(2,0) \left|2,0\right\rangle \left\langle 2,0\right|_{A,B} + P(0,2) \left|0,2\right\rangle \left\langle 0,2\right|_{A,B} \\ & P(1,1) \left|1,1\right\rangle \left\langle 1,1\right|_{A,B} + ...\end{aligned} \tag{2.18}$$

Applying the transformation due to the two beam splitters to the state results in:

$$\left|0,1\right\rangle \left\langle 0,1\right|_{A,B} \rightarrow (1-R^2) \left|0100\right\rangle \left\langle 0100\right| + R^2 \left|0001\right\rangle \left\langle 0001\right| \tag{2.19a}$$

$$\left|1,0\right\rangle \left\langle 1,0\right|_{A,B} \rightarrow (1-R^2) \left|1000\right\rangle \left\langle 1000\right| + R^2 \left|0010\right\rangle \left\langle 0010\right| \tag{2.19b}$$

$$\begin{aligned}\left|1,1\right\rangle \left\langle 1,1\right|_{A,B} \rightarrow & (1-R^2)^2 \left|1100\right\rangle \left\langle 1100\right| + R^4 \left|0011\right\rangle \left\langle 0011\right| + \\ & (1-R^2)R^2 \left|1001\right\rangle \left\langle 1001\right| + (1-R^2)R^2 \left|0110\right\rangle \left\langle 0110\right|\end{aligned} \tag{2.19c}$$

Die approbierte gedruckte Originalversion dieser Diplomarbeit ist an der TU Wien Bibliothek verfügbar
The approved original version of this thesis is available in print at TU Wien Bibliothek.
TU Bibliothek Your knowledge hub WIEN

$$\begin{aligned}|0,2\rangle\langle 0,2|_{A,B} \rightarrow &(1-R^2)^2 |0200\rangle\langle 0200| + R^4 |0002\rangle\langle 0002| \\ &2(1-R^2)R^2 |0101\rangle\langle 0101|\end{aligned} \tag{2.19d}$$

$$\begin{aligned}|2,0\rangle\langle 2,0|_{A,B} \rightarrow &(1-R^2)^2 |2000\rangle\langle 2000| + R^4 |0020\rangle\langle 0020| \\ &2(1-R^2)R^2 |1010\rangle\langle 1010|\end{aligned} \tag{2.19e}$$

Note, that again the labels where left out, but the states are from the form of $|ijkl\rangle_{A,B,Dem_A,Dem_B}$. As already indicated in [8], the demons action does not change the photon distribution between the two modes. However, modeling the mode swapping by the demon via substitution and considering the fact that $P(n,m) = P(m,n)$ when $R = 1/\sqrt{2}$ results in the output state (with $|ijkl\rangle_{A,B,Dem_A,Dem_B}$) below:

$$\begin{aligned}\rho_{out} =& P(0,0)|0000\rangle\langle 0000| + P(0,1)[(1-R^2)(|0100\rangle\langle 0100| + \\ &|1000\rangle\langle 1000|) + R^2|0001\rangle\langle 0001| + |0010\rangle\langle 0010|]+ \\ &P(1,1)[(1-R^2)^2|1100\rangle\langle 1100| + R^2(1-R^2)(|0101\rangle\langle 0101| + \\ &|0110\rangle\langle 0110|) + R^4|0011\rangle\langle 0011|] + P(0,2)[(1-R^2)^2(|2000\rangle\langle 2000| + \\ &|0200\rangle\langle 0200|) + R^4(|0020\rangle\langle 0020| + |0002\rangle\langle 0002|)+ \\ &2R^2(1-R^2)(|1010\rangle\langle 1010| + |1001\rangle\langle 1001|)]\end{aligned} \tag{2.20}$$

The probability of recording a detection event in detector D_A (D_B) is

$$\begin{aligned}P_A =& P(0,1)(1-R^2) + P(1,1)(1-R^2)^2 + \\ &P(0,2)[(1-R^2)^2 + 4R^2(1-R^2)]\end{aligned} \tag{2.21a}$$

$$\begin{aligned}P_B =& P(0,1)(1-R^2) + P(0,2)(1-R^2)^2 + \\ &P(1,1)[(1-R^2)^2 + 2R^2(1-R^2)]\,,\end{aligned} \tag{2.21b}$$

from which we calculate the photon number difference $\Delta N = \Gamma(P_A - P_B)$ as

$$\begin{aligned}\Gamma(P_A - P_B) &= 2R^2(1-R^2)(P(0,2) - P(1,1)) \\ &= 0\,.\end{aligned} \tag{2.22}$$

When substituting $P(0,1)$ and $P(1,1)$ with $R = 1\sqrt{2}$ in their explicit expression from Eq. 2.10 one can clearly see that Eq. 2.22 equals zero. Moreover,

$$\frac{\Delta N}{N} = 0 \tag{2.23}$$

independent on the amount of information (reflectivity of MD's beam splitter) the demon receives.

Die approbierte gedruckte Originalversion dieser Diplomarbeit ist an der TU Wien Bibliothek verfügbar
The approved original version of this thesis is available in print at TU Wien Bibliothek.
TU Bibliothek Your knowledge hub WIEN

Die approbierte gedruckte Originalversion dieser Diplomarbeit ist an der TU Wien Bibliothek verfügbar
The approved original version of this thesis is available in print at TU Wien Bibliothek.

Correlated Thermal States

We have shown that certain correlations prevent the demon from creating an imbalance in the photon number, whereas others can increase the MD's 'power'. To probe that, we use a type-II spontaneous parametric down-conversion source to generate a correlated thermal state. The experimental configuration can be seen in Fig. 3.1 b). In SPDC (see 2.2.3), photons are always emitted in pairs. However, it is well known, that each mode is in a thermal state by itself [17]. Such a state is given by

$$|\Psi\rangle_{corr} = \frac{1}{\cosh s} \sum_{n=0}^{\infty} (\tanh s)^n \, |n,n\rangle_{A,B} \ , \tag{2.24}$$

where s is the squeezing parameter [12]. Since we always operate in the low photon number regime, we will also here consider only the up to two photon terms:

$$|\Psi\rangle_{corr} \approx \frac{1}{1-\frac{1}{s^2}} \, |0,0\rangle_{A,B} + \frac{s}{1-\frac{1}{s^2}} \, |1,1\rangle_{A,B} + ... \tag{2.25}$$

Until now, we didn't need to consider losses, since losing a photon from a thermal state still results in a thermal state. However, for this type of state losses are determinantal for the demons 'power'. Therefore, we model loss as a beam splitter with a probability of ϵ^2 to transmit photons in mode A (B) and $(1-\epsilon^2)$ to reflect light in mode l_A (l_B), where latter indicates the photon losses. (e.g. $|1\rangle_A \rightarrow \epsilon \, |1,0\rangle_{A,l_a} + \sqrt{1-\epsilon^2} \, |0,1\rangle_{A,l_a}$) Hence, Eq. 2.25 transforms to

$$\begin{aligned} |\Psi\rangle_{corr} \approx & \frac{1}{1-\frac{1}{s^2}} \, |0000\rangle_{A,B,l,l_B} + \\ & \frac{s\epsilon\sqrt{1-\epsilon^2}}{1-\frac{1}{s^2}} (|1001\rangle_{A,B,l,l_B} + |0110\rangle_{A,B,l,l_B}) \\ & \frac{s\epsilon^2}{1-\frac{1}{s^2}} \, |1100\rangle_{A,B,l,l_B} + \frac{s(1-\epsilon^2)}{1-\frac{1}{s^2}} \, |0011\rangle_{A,B,l_A,l_B} \end{aligned} \tag{2.26}$$

When now applying the demon's beam splitters to the state, we arrive at

$$
\begin{aligned}
|\Psi\rangle_{corr} \approx & \frac{1}{1-\frac{1}{s^2}} |000000\rangle \\
& \frac{s\epsilon\sqrt{1-\epsilon^2}}{1-\frac{1}{s^2}}[R(|001001\rangle + |000110\rangle) + \sqrt{1-R^2}(|100001\rangle + |010010\rangle)] \\
& \frac{s\epsilon^2}{1-\frac{1}{s^2}}[R\sqrt{1-R^2}(|011000\rangle + |100100\rangle)+ \\
& (1-R^2)\,|110000\rangle + R^2\,|001100\rangle]+ \\
& \frac{s(1-\epsilon^2)}{1-\frac{1}{s^2}} |000011\rangle \ ,
\end{aligned}
\tag{2.27}
$$

where the states are of the form of $|ijklmn\rangle_{D_A,D_B,Dem_A,Dem_B,l_A,l_B}$. Finally, the demon uses the obtained information to swap the modes when a photon is detected at detector Dem_A, which results in $|i,j,1,0,0,0\rangle \rightarrow |j,i,1,0,0,0\rangle$. This is illustrated in Fig. 2.3 c), g) by the red photon in mode Dem_A and the blue photon in mode B. Applying this operation to our state from Eq. 2.27 results in:

$$
\begin{aligned}
|\Psi\rangle_{out} \approx & \frac{1}{1-\frac{1}{s^2}} |000000\rangle \\
& \frac{s\epsilon\sqrt{1-\epsilon^2}}{1-\frac{1}{s^2}}[R(|100001\rangle + |000110\rangle) + \sqrt{1-R^2}(|100001\rangle + |010010\rangle)] \\
& \frac{s\epsilon^2}{1-\frac{1}{s^2}}[R\sqrt{1-R^2}(|101000\rangle + |100100\rangle)+ \\
& (1-R^2)\,|110000\rangle + R^2\,|001100\rangle]+ \\
& \frac{s(1-\epsilon^2)}{1-\frac{1}{s^2}} |000011\rangle
\end{aligned}
\tag{2.28}
$$

Once again, we calculate the probabilities for detector D_A (D_B) to click:

$$P_A = \frac{s^2}{(1-\frac{1}{s^2})^2}[\epsilon^2(1-\epsilon^2)(1-R^2) + \epsilon^4(1-R^2)^2 + 2\epsilon^4 R^2(1-R^2)] \tag{2.29a}$$

$$P_B = \frac{s^2}{(1-\frac{1}{s^2})^2}[\epsilon^2(1-\epsilon^2)(1-R^2) + \epsilon^4(1-R^2)^2] \tag{2.29b}$$

Die approbierte gedruckte Originalversion dieser Diplomarbeit ist an der TU Wien Bibliothek verfügbar
The approved original version of this thesis is available in print at TU Wien Bibliothek.
TU Bibliothek Your knowledge hub WIEN

As with the other states above, we calculate the photon number difference ΔN between the modes:

$$\Delta N = \Gamma \frac{s^2}{(1-\frac{1}{s^2})^2} 2\epsilon^4 R^2 (1-R^2) \tag{2.30}$$

In order to classify the 'power of MD' we will again calculate the demons effect per photon $\Delta N/N$. However, for the correlated thermal state we can express our figure of merit for the demon also as $\Delta N/C$, which is the demon's effect per photon pair. Here, C is the total number of coincidental events detected. For calculating the former and normalize by the input singles rate, we can first of all express from Eq. 2.26 the probability for detector D_A (or D_B) to click as $\frac{s^2}{(1-\frac{1}{s^2})^2}\epsilon^2$. Repeating the experiment Γ times gives us the input singles rate $N = \Gamma \frac{s^2}{(1-\frac{1}{s^2})^2}\epsilon^2$. Thus,

$$\frac{\Delta N}{N} = 2\epsilon^2 R^2 (1-R^2)\,. \tag{2.31}$$

Examining Eq. 2.26 lets us interpret ϵ^2 also as the coupling efficiency, meaning that it is the ratio of the measured coincidences C to the singles rate before the demon is considered. A lower coupling efficiency leads to reduced the correlations between the modes. Since the 'MD's power' is dominated by the correlations and not anymore by the thermal statistics of the light, the demon is less effective. To emphasize this more, we will also calculate the effect of the demon per photon pair.

From Eq. 2.26 we obtain the probability $P_{AB} = \frac{s^2}{(1-\frac{1}{s^2})^2}\epsilon^4$ to detect a photon pair before the demon acts and hence, the incoming coincidence rate is $C = \Gamma P_{A,B}$. This leads us to the demons effect per photon pair:

$$\frac{\Delta N}{C} = 2R^2(1-R^2) \tag{2.32}$$

We can see, that the new constructed figure of merit is no longer dependent on the coupling efficiency ϵ^2 and thus indicates the ideal effect of the demon. Eq. 2.32 also reveals that the 'demon power' is the highest for a splitting ratio of the beam splitters of 50%.

Anti-Correlated Thermal States

Finally we want to discuss the photonic MD for an anti-correlated thermal state as input, which was already proposed in [8]. To prepare such a state, we perform Hong-Ou-Mandel interference [12] in order to generate a two-photon NOON-state (see Ch. 2.2.4). The higher-order terms in the SPDC process

Die approbierte gedruckte Originalversion dieser Diplomarbeit ist an der TU Wien Bibliothek verfügbar
The approved original version of this thesis is available in print at TU Wien Bibliothek.
TU Bibliothek Your knowledge hub WIEN

will not be exactly in a NOON-state, more like in a so called Holland-Burnett state [18]. However, since we operate in the low-photon number regime, the higher order modes are negligible and our state is almost identical to the one proposed in [8].

In order to calculate our figure of merit, we start by expressing the state as

$$\begin{aligned}|\Psi\rangle_{anti-corr} =& \frac{1}{1-\frac{1}{s^2}}|0,0\rangle_{A,B} + \\ & \frac{s}{1-\frac{1}{s^2}}\left(\frac{v}{\sqrt{2}}(|2,0\rangle_{A,B}+|0,2\rangle_{A,B})+\sqrt{1-v^2}\,|1,1\rangle_{A,B}\right),\end{aligned} \tag{2.33}$$

where s is again the squeezing parameter of the SPDC source and v is the visibility of the HOM-dip. Meaning that with probability $\sqrt{1-v^2}$ the two incoming photons don't bunch into one of the modes. Again we will model loss as a beam splitter, which results for the two-photon terms in $|2\rangle_A \rightarrow \epsilon^2\,|2,0\rangle_{A,l_A} + (1-\epsilon^2)\,|0,2\rangle_{A,l_A} + \sqrt{2}\epsilon\sqrt{1-\epsilon^2}\,|1,1\rangle_{A,l_A}$. The same applies for mode B. Applying the demons beam splitters results in a very similar transformation, just that ϵ is replaced with the reflection amplitude R and the mode labeling is $|i,j\rangle_{A,Dem_A}$. Again, the same applies for mode B.

Now, the demon swaps modes if a photon gets detected in Dem_B, since it is more likely, that there is another photon in mode B. This is graphically represented by the blue and the red photon in Fig. 2.3 d), h). Applying all those transformations to the state of Eq. 2.33 results in:

$$\begin{aligned}|\Psi\rangle_{out} =& \frac{1}{1-\frac{1}{s^2}}|000000\rangle + \\ & \frac{s}{1-\frac{1}{s^2}}\sqrt{1-v^2}\Big[\epsilon^2(1-R^2)\,|110000\rangle + \epsilon^2R^2\,|001100\rangle + \\ & \epsilon^2R\sqrt{1-R^2}(|011000\rangle+|010100\rangle)+\epsilon\sqrt{1-\epsilon^2}\sqrt{1-R^2}(|100001\rangle + \\ & |010010\rangle)+\epsilon\sqrt{1-\epsilon^2}R(|001001\rangle+|000110\rangle)+(1-\epsilon^2)\,|000011\rangle\Big]+ \\ & \frac{s}{1-\frac{1}{s^2}}\frac{v}{\sqrt{2}}\Big[\epsilon^2(1-R^2)(|200000\rangle+|020000\rangle)+\epsilon^2R^2(|002000\rangle + \\ & |000200\rangle)+\sqrt{2}\epsilon^2R\sqrt{1-R^2}(|101000\rangle+|100100\rangle)+ \\ & \sqrt{2}\epsilon\sqrt{1-\epsilon^2}\sqrt{1-R^2}(|100010\rangle+|010001\rangle)+ \\ & \sqrt{2}\epsilon\sqrt{1-\epsilon^2}R(|001010\rangle+|000101\rangle)+(1-\epsilon^2)(|000020\rangle+|000002\rangle)\Big]\end{aligned} \tag{2.34}$$

Die approbierte gedruckte Originalversion dieser Diplomarbeit ist an der TU Wien Bibliothek verfügbar
The approved original version of this thesis is available in print at TU Wien Bibliothek.
TU Bibliothek Your knowledge hub WIEN

The state labels were again left off, but they are $|ijklmn\rangle_{D_A,D_B,Dem_A,Dem_B,l_A,l_B}$. From Eq. 2.34 the probability for recording a detection event on detector D_A (D_B) results in:

$$P_A = \frac{s}{1-\frac{1}{s^2}}\sqrt{1-v^2}(\epsilon^2(1-R^2)+\epsilon\sqrt{1-\epsilon^2}\sqrt{1-R^2})+ \frac{s}{1-\frac{1}{s^2}}\frac{v}{\sqrt{2}}(\epsilon^2(1-R^2)+2\sqrt{2}\epsilon^2 R\sqrt{1-R^2}+\sqrt{2}\epsilon\sqrt{1-\epsilon^2}\sqrt{1-R^2}) \tag{2.35a}$$

$$P_B = \frac{s}{1-\frac{1}{s^2}}\sqrt{1-v^2}(\epsilon^2(1-R^2)+2\epsilon^2 R\sqrt{1-R^2}+\epsilon\sqrt{1-\epsilon^2}\sqrt{1-R^2})+ \frac{s}{1-\frac{1}{s^2}}\frac{v}{\sqrt{2}}(\epsilon^2(1-R^2)+\sqrt{2}\epsilon\sqrt{1-\epsilon^2}\sqrt{1-R^2})\,. \tag{2.35b}$$

The photon number difference can be calculated from the probabilities P_A and P_B as

$$\Delta N = \Gamma\frac{s^2}{(1-\frac{1}{s^2})^2}2(2v^2-1)\epsilon^4 R^2(1-R^2)\,. \tag{2.36}$$

We can see that Eq. 2.36 differs from Eq. 2.30 only by an additional factor of $(2v^2-1)$. Hence, the ideally the demon should perform the same for both states in the low-photon limit. In practice though, the imperfect HOM visibility reduces the 'power of MD' compared to the correlated state. Finally, we will construct our figure of merit by normalizing once by the incoming singles rate N and once by the incoming coincidence rate C. This results in

$$\frac{\Delta N}{N} = 2\epsilon^2(2v^2-1)R^2(1-R^2) \tag{2.37}$$

and

$$\frac{\Delta N}{C} = 2(2v^2-1)R^2(1-R^2)\,. \tag{2.38}$$

Again the coupling efficiency ϵ^2 drops out when normalizing by the coincidences.

We performed the photonic Maxwell's Demon experiment with all the states introduced above. The experimental results are presented in Ch. 4.1.

2.4 Quantum Switch with Time-Bin encoded Qubits

In this section the fundamental principle of the so called quantum SWITCH is explained. Also, we introduce a mathematical object, known as the 'causal

Die approbierte gedruckte Originalversion dieser Diplomarbeit ist an der TU Wien Bibliothek verfügbar
The approved original version of this thesis is available in print at TU Wien Bibliothek.
TU Bibliothek Your knowledge hub WIEN

witness', which is used to verify the indefinite causal structure prepared by the SWITCH. Finally, the concept of the process matrix is presented as well as how it can be determined experimentally.

2.4.1 The n-SWITCH Operation

It is well known, that quantum mechanics allows one to prepare superpositions of different quantum states, which is fundamental for creating quantum bits (Qubit). Quantum computation can lead to a computational speed-up over classical computers by sending qubits through quantum circuits, where gate operations are performed on the quantum state [24]. One way to determine the performance of a quantum algorithm is the query complexity, which is a measure for how often a quantum gate is queried [4]. Since in photonic quantum computing a gate corresponds to a physical set of waveplates or an interferometer, it is convenient to keep the number of gates used to a minimum. The classic concept of causality ensures that all processes run one after the other in a temporally defined order. However, causality is not as straight forward in quantum mechanics. In Ref. [25] the first process with an indefinite causal order was proposed and first experimentally verified in [5]. This protocol is known as the quantum SWITCH, in which a superposition of the order of different quantum gates is prepared. The action applied to the gates is called the n-SWITCH operation, where n is the number of quantum gates involved.

Recently it has been shown, that the n-SWITCH operation can outperform specific quantum algorithms with a defined causal structure in their query complexity. They propose a causal algorithm, which solves a specific problem with $\mathcal{O}(n\log(n))$ gate queries, while for solving the same problem with the n-SWITCH operation the query complexity scales only with $\mathcal{O}(n)$ [26]. The computational problem of interest is the following. There are two parties, Alice and Bob (hence, n=2) who can perform unitary gate operations U_1 and U_2 on a quantum state. The only knowledge about the gates, is that they ether commute $[U_1, U_2] = 0$ or anti-commute $\{U_1, U_2\} = 0$. To determine which statement is true, is the computational task to solve. The quantum SWITCH can, by means of a control qubit $|\Psi\rangle_C$, coherently control the order in which the gates are applied on a target qubit $|\Psi\rangle_T$. This process is visualized in Fig. 2.4.

Die approbierte gedruckte Originalversion dieser Diplomarbeit ist an der TU Wien Bibliothek verfügbar
The approved original version of this thesis is available in print at TU Wien Bibliothek.
TU Bibliothek Your knowledge hub WIEN

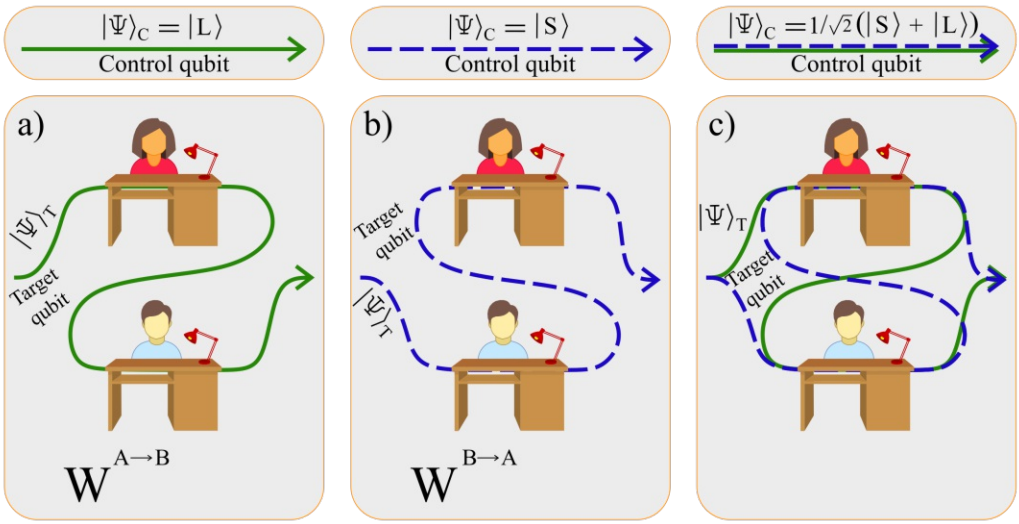

Figure 2.4: This figure visualizes the quantum n-SWITCH operation for $n = 2$. **a)** If the control qubit is in the state $|L\rangle_C$, Alice applies her gate operation before Bob on the target qubit. **b)** Whereas, if the control qubit is in the state $|S\rangle_C$, Bob will act before Alice. **c)** Since the control qubit can also be in a superposition of the two states $|\Psi\rangle_C = 1/\sqrt{2}(|S\rangle + |L\rangle)$, the target qubit $|\Psi\rangle_T$ sees both orders. Meaning that Alice acts before Bob and Bob acts before Alice. In this way the causal order of the two gates is indefinite.

Mathematically, this process can be expressed as seen below. We first prepare the input state

$$|\Psi\rangle_{in} = \frac{1}{\sqrt{2}}(|S\rangle_C + |L\rangle_C)\,|\Psi\rangle_T \ , \tag{2.39}$$

where $|\Psi\rangle_T$ is an arbirtrary polarization state acting as the target state. Applying now the quantum SWITCH operation to Eq. 2.39 results in

$$|\Psi\rangle = \frac{1}{\sqrt{2}}\,|S\rangle_C\, AB\,|\Psi\rangle_T + \frac{1}{\sqrt{2}}\,|L\rangle_C\, BA\,|\Psi\rangle_T \ . \tag{2.40}$$

Here, A and B represent the gate operations applied by Alice and Bob respectively. Finally, measuring the state of the control qubit in the diagonal basis lets us decide if the two unitary gates commute or anti-commute. The output states can then be written as

$$\begin{aligned} |\Psi\rangle_{out} =& \frac{1}{2}(|S\rangle_C + |L\rangle_C)AB\,|\Psi\rangle_T + \frac{1}{2}(|S\rangle_C - |L\rangle_C)BA\,|\Psi\rangle_T \\ =& \frac{1}{2}\,|S\rangle_C\,\{A,B\}\,|\Psi\rangle_T + \frac{1}{2}\,|L\rangle_C\,[A,B]\,|\Psi\rangle_T \ , \end{aligned} \tag{2.41}$$

Die approbierte gedruckte Originalversion dieser Diplomarbeit ist an der TU Wien Bibliothek verfügbar
The approved original version of this thesis is available in print at TU Wien Bibliothek.
TU Bibliothek Your knowledge hub WIEN

where $[A, B]$ and $\{A, B\}$ are the commutator and anti-commutator of A and B, respectively. Depending on if the gates commute or anti-commute, one of the terms in Eq. 2.41 will always equal zero. Hence, if we measure the control qubit in $|S\rangle_C$ ($|L\rangle_C$) we know that the gates commute (anti-commute).

This task was first experimentally realized in 2014 by Procopio *et al.*, where they encoded their control qubit in the path degree of freedom of the photon. Whereas, in this work we use time-bin encoding (see Ch. 2.4.2) for our qubit, which was already indicated by the control qubit states $|S\rangle_C$ and $|L\rangle_C$, where $|S\rangle_C$ is short and $|L\rangle_C$ long.

2.4.2 Qubit Encoding

In classical computation the 'bit' is a fundamental necessity in order to encode and process information. Such a classical 'bit' can occupy two different states, either '0' or '1'. Quantum computation and quantum information are built on an analogous concept. In contrast to the classical 'bit', quantum mechanics allows one to prepare a superposition of the two classical states '0' and '1'. Such a state is then called a quantum bit, or qubit, and is represented as

$$|\Psi\rangle = \alpha\,|0\rangle + \beta\,|1\rangle \ , \tag{2.42}$$

where α and β are complex numbers [24]. When a measurement is performed, the wave function collapses and we measure the qubit with probability $|\alpha|^2$ in state $|0\rangle$ and with probability $|\beta|^2$ in state $|1\rangle$. Since these are probabilities, they must always fulfill the condition $|\alpha|^2+|\beta|^2 = 1$. Qubits can be realized in many different physical systems. In following we will present three common techniques to implement qubits in a photonic domain.

A simple way to prepare a photon in a qubit state is to encode the superposition in two different spatial modes. This is often referred as 'dual-rail' representation [24]. This can be realized by simply sending a photon on a beam splitter. For example, if the photon is transmitted, we say it is in the state $|0\rangle$. On the other hand, if the photon gets reflected, it is in the state $|1\rangle$. The splitting ratio of the beam splitter determines then the complex amplitudes α and β.

Furthermore, a photon based qubit can also be encoded in the photons polarization. We use this kind of encoding for our 'target qubit' in the quantum SWITCH. One way to prepare such a state is by means of a SPDC single-photon source in a Sagnac configuration [11], as we have used for both experiments in this work. In this source a sagnac loop is pumped in one direction. Since the down-conversion process is type-II, two photons, one

Die approbierte gedruckte Originalversion dieser Diplomarbeit ist an der TU Wien Bibliothek verfügbar
The approved original version of this thesis is available in print at TU Wien Bibliothek.
TU Bibliothek Your knowledge hub WIEN

with horizontal and one with vertical polarization, are generated. If now the horizontally polarized photon is detected in the transmitted port of the polarizing beam splitter (PBS), we know that there is a second photon with vertical polarization in the reflected output of the PBS. By sending this photon through a $\lambda/4$- waveplate (QWP) and a $\lambda/2$-waveplate (HWP), one can prepare any arbitrary superposition of the form

$$|\Psi\rangle = \alpha\,|H\rangle + \beta\,|V\rangle\ , \tag{2.43}$$

where $|H\rangle$ ($|V\rangle$) represents the state $|0\rangle$ ($|1\rangle$) from Eq. 2.42 [21].

Another way for preparing a photonic qubit is time-bin encoding. To do so, a single photon is send into an unbalanced Mach-Zehnder interferometer (MZI) with one path longer than the other. If the photon takes the short path, we label the state $|S\rangle$, which corresponds to $|0\rangle$ in Eq. 2.42. Whereas, if it takes the long path of the MZI, the photon is in the state $|L\rangle$ and hence, represents $|1\rangle$ in Eq. 2.42. Typically the beam splitters of the MZI are balanced and hence, the photon has an equal probability of taking ether path. This leads to the photon being in a coherent superposition of both states and can be written as [27]

$$|\Psi\rangle = \frac{1}{\sqrt{2}}(|S\rangle + |L\rangle)\,. \tag{2.44}$$

Since the beam splitters of the MZI have a balanced splitting ratio, the coefficients are $\alpha = \beta = 1/\sqrt{2}$. Performing a measurement on the qubit in the computational basis $\{|S\rangle\,, |L\rangle\}$ can be simply done by measuring the time of arrival. Whereas for measuring in other basis, e.g. in the diagonal basis $\{|+\rangle\,, |-\rangle\}$, the time-bins have to be brought together using another (or in our case the same) MZI [27]. For the quantum switch experiment we choose to encode the 'control qubit' in time-bins.

2.4.3 Polarization single-Qubit Gates

In Ch. 2.4.1 the functional concept of the 2-SWITCH operation was explained, in which two parties, Alice and Bob perform gate operations on a polarization qubit. As already mentioned above, on a photonic platform, polarization gates can be realized via waveplates. Since we implemented two different kinds of polarization qubit gates, the concept of these types is explained below.

Unitary Gate

Lets remember from Ch. 2.4.2, that a qubit can be described by the quantum

Die approbierte gedruckte Originalversion dieser Diplomarbeit ist an der TU Wien Bibliothek verfügbar
The approved original version of this thesis is available in print at TU Wien Bibliothek.
TU Bibliothek Your knowledge hub WIEN

state $|\Psi\rangle = \alpha\,|0\rangle + \beta\,|1\rangle$. It turns out, that the only constraint for a quantum gate is that all operations on the qubit preserve the norm $|\alpha|^2 + |\beta|^2 = 1$ of the state. The consequence of this is that the two by two matrices describing single-qubit transformations must be unitary [24]. These matrices, U_{2x2}, are all united by the two-dimensional special unitary group SU(2). Since SU(2) is a three parameter group, it turns out that a set of two $\lambda/4$- and one $\lambda/2$-waveplate can realize any transformation of this group [28]. In this work we realize the unitary gates in the common combination of $\lambda/4 - \lambda/2 - \lambda/4$ wavepaltes. The resulting unitary matrix can be obtained by multiplying the corresponding Jones matrices for the waveplates, which can be written as

$$J_{\lambda/4} = e^{-i\frac{\pi}{4}} \begin{pmatrix} \cos^2(\theta) + i\sin^2(\theta) & (1-i)\sin(\theta)\cos(\theta) \\ (1-i)\sin(\theta)\cos(\theta) & \sin^2(\theta) + i\cos^2(\theta) \end{pmatrix} \tag{2.45}$$

and

$$J_{\lambda/2} = e^{-i\frac{\pi}{2}} \begin{pmatrix} \cos^2(\theta) - \sin^2(\theta) & 2\sin(\theta)\cos(\theta) \\ 2\sin(\theta)\cos(\theta) & \sin^2(\theta) - \cos^2(\theta) \end{pmatrix}, \tag{2.46}$$

where θ is the angle between the fast axis and the x-axis [21].

Measurement/Re-Preparation Channel

In addition to the computational problem of determining whether two unitary operators commute or anti-commute, we also want to measure a so called 'causal witness' (which will be explicitly explained in Ch. 2.4.4) on the SWITCH. Since it turns out, that the significance of the witness is much higher with measurement/re-preparation channels, we also want to implement those in the quantum SWITCH.

The underlying concept of this different type of channel is that of projective measurements. In contrast to the measurement of a photon with a detector, in which the incident particle is destroyed, with a projective measurement the photon is not destroyed but collapsed onto a certain polarization state. In practice this can be done with a polarization filter. Mathematically, this can be formulated as

$$|\Psi\rangle \xrightarrow[\text{projective}]{\text{measurement}} |\xi\rangle = \frac{\hat{P}(\xi)\,|\Psi\rangle}{\sqrt{\langle\Psi|\,\hat{P}(\xi)\,|\Psi\rangle}}, \tag{2.47}$$

where the quantum state $|\Psi\rangle$ gets projected on the state $|\xi\rangle$. $\hat{P}(\xi) = |\xi\rangle\langle\xi|$ is the so called projector on the state $|\xi\rangle$ and the square root term in the denominator of Eq. 2.47 is due to normalization of the new state [12]. As an example, when considering a photon in the polarization state $|\theta\rangle = \cos(\theta)\,|H\rangle + \sin(\theta)\,|V\rangle$ (with θ being the angle between the polarization

Die approbierte gedruckte Originalversion dieser Diplomarbeit ist an der TU Wien Bibliothek verfügbar
The approved original version of this thesis is available in print at TU Wien Bibliothek.
TU Bibliothek Your knowledge hub WIEN

vector and the horizontal axis) which approaches a polarizer oriented horizontally, the projector can be written as $\hat{P}(H) = |H\rangle\langle H|$ and the state $|\theta\rangle$ is collapsed, with probability $\cos^2(\theta)$ to $|H\rangle$ [12].

With the knowledge gained about projective measurements, we can now present the concept of the measurement/re-preparation channels that were implemented in our setup. Physically they are realized by a $\lambda/4$- and a $\lambda/2$-waveplate followed by a polarizer in horizontal orientation and another set of $\lambda/4$- and a $\lambda/2$-waveplates. Together with the first sequence of waveplates, which form unitary pre-measurement operators and the the horizontally oriented polarization filter, Alice and Bob can perform projective measurements in the $\{|H\rangle, |V\rangle\}$ basis. After the incoming polarization state is projected on $|H\rangle$, a superposition state can be re-prepared by the second sequence of waveplates, which again form unitary operators. Note that, a set of two waveplates also performs unitary operations on the polarization state. The only difference to the unitary gate explained above is that they don't cover all transformations of SU(2).

2.4.4 The Causal Witness

Analogous to the description of quantum states using density matrices, quantum processes can be described using process matrices. A causal witness is a theoretical tool to determine weather a such a process is causally separable or not. To understand its concept, we first consider an analogous object, which is the entanglement witness [29]. Therefore, we first consider a composite quantum system, which lives in a Hilbert space $\mathcal{H}_\mathrm{A} \otimes \mathcal{H}_\mathrm{B}$. If the state of this system can be written as a product state $|\Psi\rangle_\mathrm{A} \otimes |\Phi\rangle_\mathrm{B}$, the system is separable and therefore not entangled. For all entangled states, ρ^ent, there exists an Hermitian operator $\hat{S}$, such that $\mathrm{Tr}\{\hat{S}\rho^\mathrm{ent}\} < 0$. For all separable states ρ^sep, $\mathrm{Tr}\{\hat{S}\rho^\mathrm{sep}\} \geq 0$. $\hat{S}$ is then called an entanglement witness.

The causal witness fulfills a very similar relation. But first, we will introduce the concept of the process matrix W, which describes causal relations between different local laboratories. Here, 'local' means that the only connection to the surrounding system is the quantum state received from outside and the state that is returned. When considering two parties, Alice and Bob who perform local operations M^A and M^B on an incoming quantum state in their laboratories, the process matrix describes how the quantum state propagates between the two parties. Note, that W is independent from the operations performed by Alice and Bob. The process matrix is graphically illustrated in Fig. 2.5 b). Performing a so called 'causal tomography' on the system lets us determine the causal relationship between the two parties [5]. For that we have to probe the system with different input states ρ_z^in, while

Die approbierte gedruckte Originalversion dieser Diplomarbeit ist an der TU Wien Bibliothek verfügbar
The approved original version of this thesis is available in print at TU Wien Bibliothek.
TU Bibliothek Your knowledge hub WIEN

Alice and Bob implement different operations $M^{\mathrm{A}}_{a,x}$ and $M^{\mathrm{B}}_{b,y}$. At the output, measurements D^{out}_d are performed. Here, a and b represent the outcomes of the specific local operations x and y executed by Alice and Bob. z determines the chosen input state and d the corresponding result of a measurement. The probability of obtaining a certain outcome for a specific configuration can be expressed by using the Choi-Jamiolkowski isomorphism as

$$p(a,b,d|x,y,z) = \mathrm{Tr}\{(\rho^{\mathrm{in}}_z \otimes M^{\mathrm{A}}_{a,x} \otimes M^{\mathrm{B}}_{b,y} \otimes D^{\mathrm{out}}_d)W\}\,, \tag{2.48}$$

with $\sum_{a,b,d} p(a,b,d|x,y,z) = 1$ for all settings x,y,z [5].

Since Eq. 2.48 is dependent on the process matrix W, we want to construct the corresponding matrix for the quantum SWITCH. The just introduced Choi-Jamiolkowski isomorphism is a convenient method for representing linear operators, which map a Hilbert space $\mathcal{H}_{\mathrm{in}}$ to $\mathcal{H}_{\mathrm{out}}$ as a state in the composite Hilbert space $\mathcal{H}_{\mathrm{in}} \otimes \mathcal{H}_{\mathrm{out}}$. The link between an output space $\mathcal{H}^{P_1}_{\mathrm{out}}$ from a party P_1 to the input space $\mathcal{H}^{P_2}_{\mathrm{in}}$ of a party P_2 can be described by the identity channel. This can be expressed as a process vector in the 'double-ket notation' [30]

$$|\mathbb{1}\rangle\rangle^{\mathcal{H}^X_{\mathrm{in/out}}\mathcal{H}^Y_{\mathrm{in/out}}} = \sum_j |j\rangle^{\mathcal{H}^X_{\mathrm{in/out}}} \otimes |j\rangle^{\mathcal{H}^Y_{\mathrm{in/out}}}\,, \tag{2.49}$$

where j forms a basis over the space [5]. With the formulation of the identity channel we can now describe an input state passing through the quantum SWITCH. Precisely the state passes first to Alice ($\mathcal{H}^A_{\mathrm{in}} \to \mathcal{H}^A_{\mathrm{out}}$), then to Bob ($\mathcal{H}^B_{\mathrm{in}} \to \mathcal{H}^B_{\mathrm{out}}$) and in the end to the output space $\mathcal{H}^{\mathrm{out}}$. This sequence can be represented by the process vector

$$\left|W^{\mathrm{A}\to\mathrm{B}}\right\rangle = |\mathbb{1}\rangle\rangle^{\mathcal{H}^{\mathrm{in}}\mathcal{H}^A_{\mathrm{in}}} |\mathbb{1}\rangle\rangle^{\mathcal{H}^A_{\mathrm{out}}\mathcal{H}^B_{\mathrm{in}}} |\mathbb{1}\rangle\rangle^{\mathcal{H}^B_{\mathrm{out}}\mathcal{H}^{\mathrm{out}}} \tag{2.50}$$

To describe the process in which Bob acts before Alice $\left|W^{\mathrm{B}\to\mathrm{A}}\right\rangle$, one just needs to switch the labels in Eq. 2.50. Note, that the introduced process vectors are independent of the specific operations Alice and Bob perform.

Together with the control qubit in the state $|\Psi\rangle_C = 1/\sqrt{2}(|S\rangle + |L\rangle)$, we can now construct the process vector of the SWITCH:

$$|W_{\mathrm{SWITCH}}\rangle = \frac{1}{\sqrt{2}}(\left|W^{\mathrm{B}\to\mathrm{A}}\right\rangle |S\rangle_C + \left|W^{\mathrm{A}\to\mathrm{B}}\right\rangle |L\rangle_C) \tag{2.51}$$

Since we only measure the state of the control qubit after the SWITCH and not the photons polarization, meaning the target qubit, we have to construct a process matrix which takes the target as an input state and returns the control qubit. This can be achieved by taking the partial trace over the target

Die approbierte gedruckte Originalversion dieser Diplomarbeit ist an der TU Wien Bibliothek verfügbar
The approved original version of this thesis is available in print at TU Wien Bibliothek.
TU Bibliothek Your knowledge hub WIEN

qubit in the output of the quantum SWITCH. Hence, the process matrix can be expressed as [5]

$$W_{SWITCH} = \mathrm{Tr}_{\mathcal{H}^{\mathrm{out}}}\{|W_{\mathrm{SWITCH}}\rangle\langle W_{\mathrm{SWITCH}}|\} \tag{2.52}$$

At the beginning of this chapter we referred to the concept of the causal witness in analogy to an entanglement witness. The condition for a process with an indefinite causal order is, that there exists a Hermitian superoperator $\hat{S}$ so that

$$\mathrm{Tr}\{\hat{S}W^{\text{n-sep}}\} < 0 \tag{2.53}$$

where $W^{\text{n-sep}}$ is an arbitrary non-separable process matrix. For all separable process matrices W^{sep}, $\mathrm{Tr}\{\hat{S}W^{\text{sep}}\} \geq 0$. $\hat{S}$ is then called a causal witness [5]. This is graphically illustrated in Fig. 2.5 a). Experimentally, a causal witness is a series of measurements in which several input states are prepared and different quantum channel operations are applied to them. Hence, we want to decompose the causal witness into those operations by using the notation of Eq. 2.48 and therefore $\hat{S}$ can be expanded to

$$\hat{S} = \sum_{a,b,d,x,y,z} \alpha_{a,b,d,x,y,z}\rho_z^{\text{in}} \otimes M_{a,x}^{\text{A}} \otimes M_{b,y}^{\text{B}} \otimes D_d^{\text{out}}\,, \tag{2.54}$$

where the coefficients $\alpha_{a,b,d,x,y,z}$ are real numbers and represent the weight of a certain measurement for the witness [5]. Hence, the causal non-separability can be calculated as

$$\mathrm{Tr}\{\hat{S}W\} = \sum_{a,b,d,x,y,z} \alpha_{a,b,d,x,y,z} p(a,b,d|x,y,z)\,. \tag{2.55}$$

From Eq. 2.55 one can see, that effectively the witness can be constructed by evaluating probabilities for the individual measurement outcomes. If $\mathrm{Tr}\{\hat{S}W_{\mathrm{SWITCH}}\} < 0$ we can say that the process performed by the quantum SWITCH shows an indefinite causal order.

Die approbierte gedruckte Originalversion dieser Diplomarbeit ist an der TU Wien Bibliothek verfügbar
The approved original version of this thesis is available in print at TU Wien Bibliothek.
TU Bibliothek Your knowledge hub WIEN

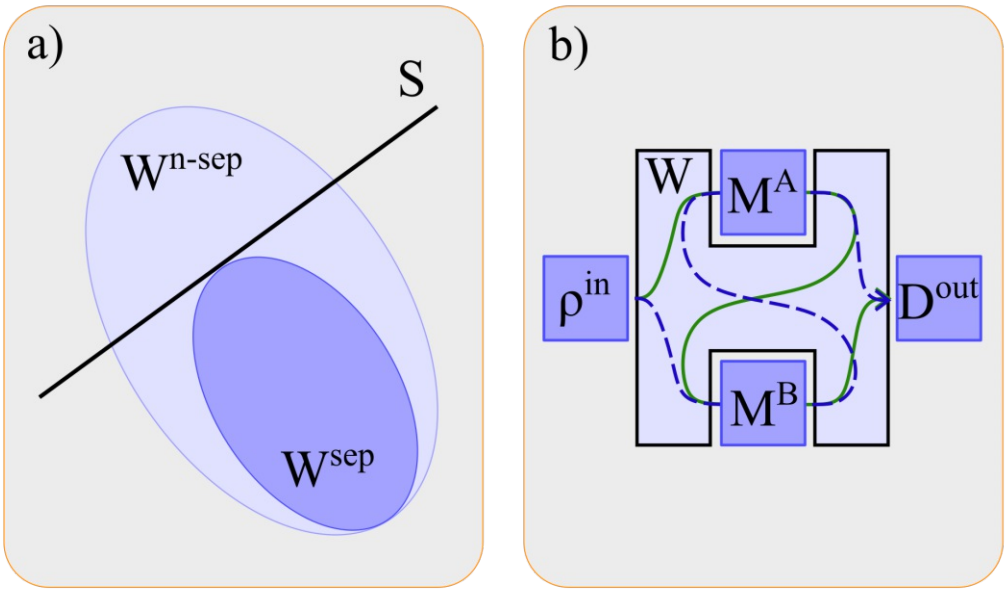

Figure 2.5: **a)** This figure illustrates the causal witness. The inner ellipse represents all causally separable process matrices W^{sep}. The black line (which is actually a hyperplane) symbolizes the causal witness $\hat{S}$, that separates all causally separable process from a corresponding non-separable process. The set of causally non-separable process matrices W^{n-sep} is represented by the outer ellipse. **b)** This figure represents the process matrix W, which is illustrated by the 'H-shaped' area. It describes how the input state ρ^{in} is routed first to Alice's local operation M^{A} an after to Bob where he performs his local operation M^{B} on the target state or vice versa. In the case of the quantum SWITCH, a superposition of both paths is present, which is conditioned on the state of the control qubit. D^{out} represents the measurement performed on the control qubit at the output of the SWITCH.

2.4.5 Quantum Process Tomography

In Ch. 2.4.4 we already mentioned the formalism of the process matrix and introduced the mathematical object of the causal witness. Here, we will go into more detail on the process matrix itself and how it can be determined experimentally using quantum process tomography. As mentioned before, the process matrix W can be seen as a counter part to the density matrix ρ which describes the dynamics of a quantum process rather than the quantum state used to probe it. It can thus describe the causal relationship between the local laboratories involved in the process. The operations performed by the individual parties, Alice and Bob, can be described through completely

Die approbierte gedruckte Originalversion dieser Diplomarbeit ist an der TU Wien Bibliothek verfügbar
The approved original version of this thesis is available in print at TU Wien Bibliothek.
TU Bibliothek Your knowledge hub WIEN

positive (CP) maps $\mathcal{M}^X : \mathcal{L}(\mathcal{H}^{\mathrm{X}}_{\mathrm{in}}) \to \mathcal{L}(\mathcal{H}^{\mathrm{X}}_{\mathrm{out}})$, which map a quantum state from an input Hilbert space $\mathcal{H}^{\mathrm{X}}_{\mathrm{in}}$ to an output space $\mathcal{H}^{\mathrm{X}}_{\mathrm{out}}$, where $\mathrm{X} \in \{\mathrm{A}, \mathrm{B}\}$ is indicating the Hilbert space of Alice or Bob [3]. Such completely positive maps can be represented by positive semi-definite matrices via the Choi-Jamiolkowski (CJ) isomorphism [31]. Hence, a general CP map $\mathcal{M}^X$ can be written as a CJ matrix as

$$M^{\mathrm{X}} := [\mathcal{I} \otimes \mathcal{M}^{\mathrm{X}}(|\mathbb{1}\rangle\rangle\langle\langle\mathbb{1}|)]^{\mathrm{T}}\,, \tag{2.56}$$

where $M^{\mathrm{X}} \in \mathcal{L}(\mathcal{H}^{\mathrm{X}}_{\mathrm{in}}) \otimes \mathcal{L}(\mathcal{H}^{\mathrm{X}}_{\mathrm{out}})$, $\mathcal{I}$ is the identity map and $|\mathbb{1}\rangle\rangle\langle\langle\mathbb{1}|$ is the process matrix constructed from the process vector from Eq. 2.49 and describes the link between the input and the output Hilbert space [3]. In words, the identity map acts on the input state, while $\mathcal{M}^{\mathrm{X}}$ acts on the output state of the operation.

Now that we can express the operations performed by Alice and Bob, we also want to represent the input state in the CJ-isomorphism. The density matrix ρ of an arbitrary quantum state $|\Psi\rangle$ is defined as $\rho = |\Psi\rangle\langle\Psi|$. In the CJ-formalism such a quantum state can be expressed as

$$\rho^{\mathrm{in}} = |\Psi\rangle\langle\Psi| \otimes \mathcal{I}\,. \tag{2.57}$$

Again, in words, the projector $|\Psi\rangle\langle\Psi|$ acts on the input, while the identity map $\mathcal{I}$ acts on the output space. It can be shown, that the output of the identity process can than be calculated as $\rho^{\mathrm{out}} = \mathrm{Tr}\{(\rho^{\mathrm{in}})^{\mathrm{T}}\,|\mathbb{1}\rangle\rangle\langle\langle\mathbb{1}|\}$. When constructing the process matrix for a general process $\mathcal{E}$ as $|\mathcal{E}\rangle\rangle\langle\langle\mathcal{E}| = \mathcal{I}_{\mathrm{in}} \otimes \mathcal{E}_{\mathrm{out}}(|\mathbb{1}\rangle\rangle\langle\langle\mathbb{1}|)$, again the output can then be calculated as $\mathcal{E}(\rho) = \mathrm{Tr}\{(\rho^{\mathrm{in}})^{\mathrm{T}}\,|\mathcal{E}\rangle\rangle\langle\langle\mathcal{E}|\}$.

Considering now again the situation from Ch. 2.4.4, where two parties, Alice and Bob, can perform different operations $M^{\mathrm{A}}_{a,x}$ and $M^{\mathrm{B}}_{b,y}$ in their local laboratories on an incoming quantum state. Again, a and b determine the outcomes of specific operations x and y. At the end of the process a measurement D^{out}_d with result d is performed. The probability of obtaining a certain outcome for a specific operation can be written as in Eq. 2.48. As already described in Ch. 2.4.4 the process vector for the case where Alice acts before Bob or vice versa can be obtained according to Eq. 2.50. To express the process vector of the quantum SWITCH, we simply need to add the control qubit as done in Eq. 2.51. Now, the probability for obtaining a certain outcome of the SWITCH can be written as

$$p(a, b, d|x, y, z) = \mathrm{Tr}\{(\rho^{\mathrm{in}}_z \otimes M^{\mathrm{A}}_{a,x} \otimes M^{\mathrm{B}}_{b,y} \otimes D^{\mathrm{out}}_d)W_{SWITCH}\} \tag{2.58}$$

Note, that the specific operations performed in the SWITCH are now fully decoupled from the process matrix. Hence, W_{SWITCH} does not depend on

Die approbierte gedruckte Originalversion dieser Diplomarbeit ist an der TU Wien Bibliothek verfügbar
The approved original version of this thesis is available in print at TU Wien Bibliothek.
TU Bibliothek Your knowledge hub WIEN

them. It also needs to be mentioned, that in this work we only performed measurements on the state of the control qubit and hence, the process matrix in Eq. 2.58 is the one from Eq. 2.52, that traces over the target qubit.

To determine the process matrix experimentally, one has to perform quantum process tomography. In order to understand this, we shall briefly review quantum state tomography. To determine an unknown quantum state $|\Psi\rangle$, an ensemble of this state is fed into a measurement device, which applies a complete set of different measurement projectors on $|\Psi\rangle$. Resulting from that, one can determine the initially unknown quantum state [24]. To describe an unknown quantum process $\mathcal{E}$, the procedure is quiet similar. Therefore, one needs to send a complete set of known input states, meaning that they form a basis over the total input Hilbert space, into the unknown process $\mathcal{E}$ and then perform state tomography on the output of this process. Out of these results, it is possible to fully evaluate the desired process matrix and with that calculate the output state of the process for any arbitrary input state [24]. In order for the estimated matrix to describe a physically valid process, it must be a complex Hermitian matrix and also satisfy the following constraints [31]:

$$W \geq 0 \tag{2.59a}$$

$$\operatorname{Tr} W = d_{\mathrm{O}} \tag{2.59b}$$

$$W = L_V(W) \tag{2.59c}$$

Here, Eq. 2.59a confines the allowed matrices to be positive-semidefinite in order to ensure only non-negative probabilities. In Eq. 2.59b is the normalization constraint, where d_{O} is the product of all output Hilbert space dimensions. In the case of our quantum SWITCH, L_V is a projector on the linear subspace $\mathcal{L} \subset \mathcal{H}_{\mathrm{in}} \otimes \mathcal{H}^{\mathrm{A}}_{\mathrm{in}} \otimes \mathcal{H}^{\mathrm{A}}_{\mathrm{out}} \otimes \mathcal{H}^{\mathrm{B}}_{\mathrm{in}} \otimes \mathcal{H}^{\mathrm{B}}_{\mathrm{out}} \otimes \mathcal{H}_{\mathrm{out}}$ and hence, Eq. 2.59c ensures that W_{SWITCH} also lives in this space. Each output Hilbert space of this subspace has dimension $d = 2$ and thus, $d_O = 8$ for our SWITCH. When W satisfies the condition above, it is in fact a valid process matrix. Considering that transferring a qubit from an input space to an output space corresponds to a 2-qubit state tomography, the process tomography performed on a two-party quantum SWITCH is equivalent to a 6-qubit tomography.

Die approbierte gedruckte Originalversion dieser Diplomarbeit ist an der TU Wien Bibliothek verfügbar
The approved original version of this thesis is available in print at TU Wien Bibliothek.
TU Bibliothek Your knowledge hub WIEN

Die approbierte gedruckte Originalversion dieser Diplomarbeit ist an der TU Wien Bibliothek verfügbar
The approved original version of this thesis is available in print at TU Wien Bibliothek.

Die approbierte gedruckte Originalversion dieser Diplomarbeit ist an der TU Wien Bibliothek verfügbar
The approved original version of this thesis is available in print at TU Wien Bibliothek.

Chapter 3

Experimental Setup

In this chapter the experimental setup of the photonic Maxwell demon and the quantum switch is presented.

3.1 Photonic Maxwell's Demon

As already mentioned in Ch. 2.3, we carried out our photonic Maxwell demon experiment with four different input states. In this section the experimental configuration of those photon sources and also the setup of the photonic Maxwell's demon will be explained. A schematic drawing of the setup is shown in Fig. 3.1.

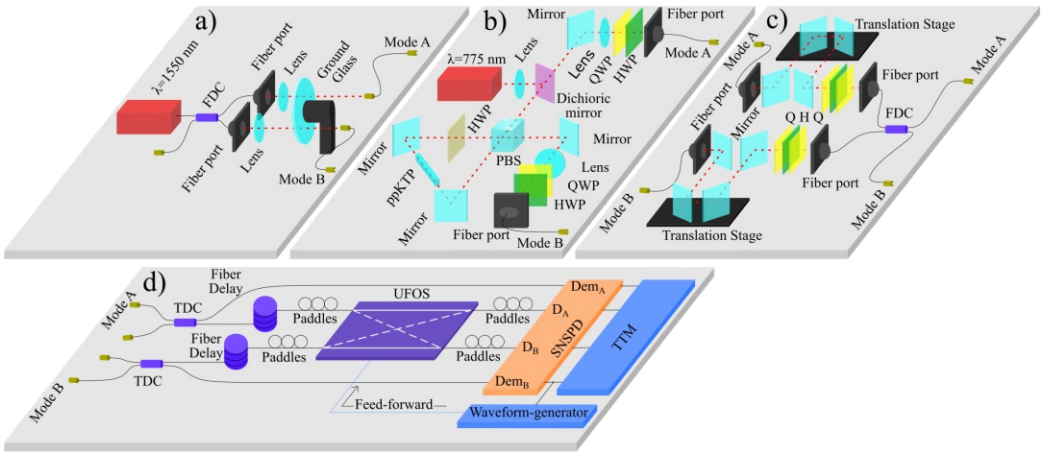

Figure 3.1: **a)** Thermal light Source, **b)** Correlated light source, **c)** anti-correlated light source (two photon NOON-state), **d)** Photonic Maxwell's Demon. Note that the acronyms used in the illustration are the same as in the text. In panel **c)**, "Q H Q" stand for a $\lambda/2$-waveplate sandwiched by two $\lambda/4$-waveplates.

The experimental configuration for generating two uncorrelated thermal states is presented in Fig. 3.1 a). Here, coherent light at a wavelength

of 1550 nm is emitted by a diode laser and propagates through a fiber directional coupler (FDC), where the two spatial single-modes A and B are prepared. Both modes are coupled into free space and their light is focused in both arms by a lens on seperate spots of a spinning ground glass (grit size 220). At this point the coherent light obtains pseudo thermal light statistics. The process of generating a photonic thermal state is explained precisely in Ch. 2.2.2. In each arm a bare fiber collects the thermal light. To verify the thermal statistics of each mode, we measure the second order coherence function $g^2(\tau)$ by use of an intensity interferometer in the Hanbury, Brown and Twiss configuration and obtain $g^2(\tau) \approx 1.95$ and a coherence time of $\tau \approx 5.42\mu$s [32].

In order to prepare two classically correlated thermal states, we split one of the thermal states generated by the scheme of Fig. 3.1 a) and let it propagate through a balanced FDC (not shown in Fig.3.1). The two outputs of the FDC realize the classical, correlated thermal modes A and B. In this work we refer to this as a split thermal state.

Fig. 3.1 b) shows a SPDC single-photon source in a Sagnac configuration [11]. A type-II periodically poled $KTiOPO_4$ (PPKTP) crystal in a Sagnac loop provides the non-linear medium for the down conversion process. For generating the pump beam, a Toptica Photonics TA Pro Laser is used, which operates in continuous wave (CW) mode at a wavelength of $\lambda = 775$ nm. Hence, photon pairs at $\lambda = 1550$ nm are generated. The modes A and B prepared by this setup are correlated thermal states (Remember from Ch. 2.3.2, unlike the correlations mentioned above, correlations generated by SPDC enhance the MD's power.). Note that, since we don't require polarization entangled photon pairs, the Sagnac loop is only pumped in one direction.

Moreover, we prepare the two down converted photons in a NOON-state to probe the MD's power with an anti-correlated thermal state. The setup shown in Fig. 3.1 c) connects to the output modes A and B from the SPDC source respectively. Each mode is coupled into free-space and propagates across a variable delay line. By that one can set the path difference undergone by the photons to zero. This leads to the required time-overlap of the photons to achieve Hong-Ou-Mandel (HOM) interference [12]. For making the photons indistinguishable in polarization, each path hosts a set of two $\lambda/4$-waveplates and a $\lambda/2$-waveplate. Finally both modes are coupled into a single-mode fiber, where they will interfere according to the HOM effect on a FDC. Since the fibers can host only a single mode, the spatial overlap is automatically given. For sustaining the maximal interference visibility, the photons need to be indistinguishable in all degrees of freedom. To achieve this condition for the photon wavelength, the PPKTP crystal's temperature

Die approbierte gedruckte Originalversion dieser Diplomarbeit ist an der TU Wien Bibliothek verfügbar
The approved original version of this thesis is available in print at TU Wien Bibliothek.
TU Bibliothek Your knowledge hub WIEN

in the SPDC source can be fine tuned using an oven. For a given crystal temperature, the photons wavelength will overlap [11].

The experimental configurations from Fig. 3.1 a)-c) all prepare two modes A and B hosting different thermal states with which we probe the MD's power. These modes are then linked via optical fibers to the two input modes of the photonic MD setup (see Fig. 3.1 d). Each mode propagates through a tuneable directional coupler (TDC). By tuning the reflection amplitude R of the TDC one can control how much information the demon can gain about the thermal states. This information is aquired through measurements at the reflected ports of the TDC with detectors Dem_A and Dem_B (both are SNSPD from PhotonSpot Inc.). The experiment is based on a 2x2 UFOS (BATi 2x2 Nanona fiber switch, response time below 60 ns). By applying the feed-forward protocol (from Ch. 2.1) conditioned on the measurement outcomes at detectors Dem_A and Dem_B, the demon can use the UFOS to route photons between mode A and B. To change the state of the UFOS we apply to it a 2.5 μs long TTL pulse. A time tagging module (UQDevices Logic16 TTM) records the photons of both modes detected at D_A and D_B. Hence, we can evaluate the photon number difference between mode A and B. Since the detection efficiency of the SNSPD is polarization dependent, both the input and output fibers of the UFOS is equipped with a fiber paddle polarization controller. Therefore, the difference in polarization between the two modes can be compensated, so that the photons always arrive with a common polarization at the detectors.

3.2 Quantum SWITCH

The second part of this work is the quantum SWITCH experiment. The photon source here is the one from Fig. 3.1 b). The newly proposed fiber-based architecture for the quantum SWITCH is illustrated in Fig. 3.2. Again, the states of the UFOS's in this setup are controlled by the feed-forward protocol from Ch. 2.1. For that, one of the down converted photons is heralded to the SNSPD. The herald signal is then used as a timing reference to start the pulse sequence applied to the UFOSs.

Die approbierte gedruckte Originalversion dieser Diplomarbeit ist an der TU Wien Bibliothek verfügbar
The approved original version of this thesis is available in print at TU Wien Bibliothek.
TU Bibliothek Your knowledge hub WIEN

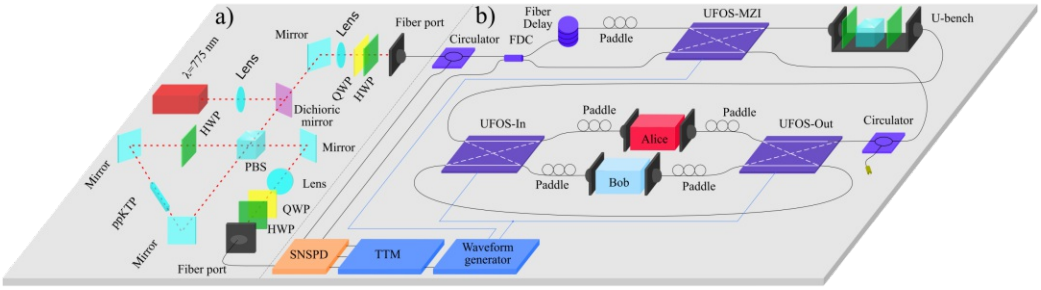

Figure 3.2: This figure illustrates the experimental setup of the quantum SWITCH. Panel **a)** shows the same SPDC single-photon source as used for the Maxwell's Demon experiment (see Fig. 3.1 b)). In panel **b)**, the quantum SWITCH is illustrated. The upper section of the figure shows the MZI, where the time-bins are created and re-combined. Below is the fiber-based architecture for the SWITCH. The individual gates, represented by 'Alice' and 'Bob', can be either unitary gates or measurement/re-preparation channels (see Ch. 2.4.3.)

Meanwhile the signal photon is coupled into the setup, where it first passes a fiber optical circulator and a balanced FDC. This is where the control qubit, encoded in time bins, is created. Therefore, one of the FDC's outputs is followed by a 150 ns fiber delay line equipped with a fiber paddle polarization controller. Both FDC output modes connect to a UFOS (labeled as UFOS-MZI in Fig. 3.2 b)). When applying the feed-forward protocol with a pulse length of 150 ns, we can route the time bins individually. Light which takes the short (long) path is refereed to the control qubit being in the state $|S\rangle$ ($|L\rangle$). Since the ground state of the UFOS is 'cross', $|S\rangle$ leaves the clockwise (cw) output of the UFOS. The feed-forward pulse changes the UFOS state to 'bar' and hence also $|L\rangle$ exits the cw output.

Next, the photon propagates through a few cm long free-space section of a fiber coupled u-bench. Here, the light passes through a polarizing beam splitter (PBS) sandwiched by two $\lambda/2$-waveplates. Adjusting the first one maximizes the photon transmission through the PBS, while the second waveplate allows to fix the state of the target qubit to any linear polarization state. This enables us to probe the SWITCH with different input states.

Now that the input state of the photon is prepared, it can enter the quantum SWITCH. The architecture is based on two more UFOS's (In & Out) and two free-space polarization gates. In this work we performed measurements on the SWITCH with both, unitary quantum gates and measurement/re-preparation channels (see Ch. 2.4.3). In the following, the path taken by the individual time-bins is explained and a graphical illustration of this procedure is shown in Fig. 3.3. First, $|S\rangle$ enters the setup and passes UFOS-In in

Die approbierte gedruckte Originalversion dieser Diplomarbeit ist an der TU Wien Bibliothek verfügbar
The approved original version of this thesis is available in print at TU Wien Bibliothek.
TU Bibliothek Your knowledge hub WIEN

the 'cross' state. Hence, gate B is applied to the target qubit $|\Psi\rangle$ ($|S\rangle\, B\, |\Psi\rangle$). Before $|L\rangle$ propagtes through UFOS-In, we apply the feed-forward protocol with a TTL pulse sequence of two high-levels and one low-level to both of the UFOS's simultaneously. Each level state of this sequence is of the length of the time-bin separation (150 ns). Hence, $|L\rangle$ passes UFOS-In in the 'bar' state, where gate A is applied to the target qubit ($|L\rangle\, A\, |\Psi\rangle$) while $|S\rangle$ transmits UFOS-Out as well in the 'bar' state and therefore loops through a fiber back to UFOS-In. Meanwhile the low-level of the pulse sequence is present, which puts both UFOS back in the 'cross' state. While in this state, $|S\rangle$ is directed to gate A ($|S\rangle\, AB\, |\Psi\rangle$) and $|L\rangle$, which comes from gate A loops now also back to UFOS-In. The second high-level of the pulse sequence sets both UFOS again in the 'bar' state. This leads to $|L\rangle$ passing now gate B ($|L\rangle\, BA\, |\Psi\rangle$), while $|S\rangle$ already leaves the quantum SWITCH. After the TTL pulse sequence is finished, both UFOS stay in their ground state ('cross') and hence, also $|L\rangle$ can leave the SWITCH. The three paths of gate A, B and the backward running loop are all matched to a photon propagation time of 150 ns. As it can be seen in Fig. 3.2, both the gates are sandwiched by two fiber paddle polarization controllers. These are used to compensate for unwanted transformations on the photons polarization according to the technique presented in appendices A. This is necessary so that the target qubit only experiences operations performed by Alice and Bob (gates A and B).

Die approbierte gedruckte Originalversion dieser Diplomarbeit ist an der TU Wien Bibliothek verfügbar
The approved original version of this thesis is available in print at TU Wien Bibliothek.
TU Bibliothek Your knowledge hub WIEN

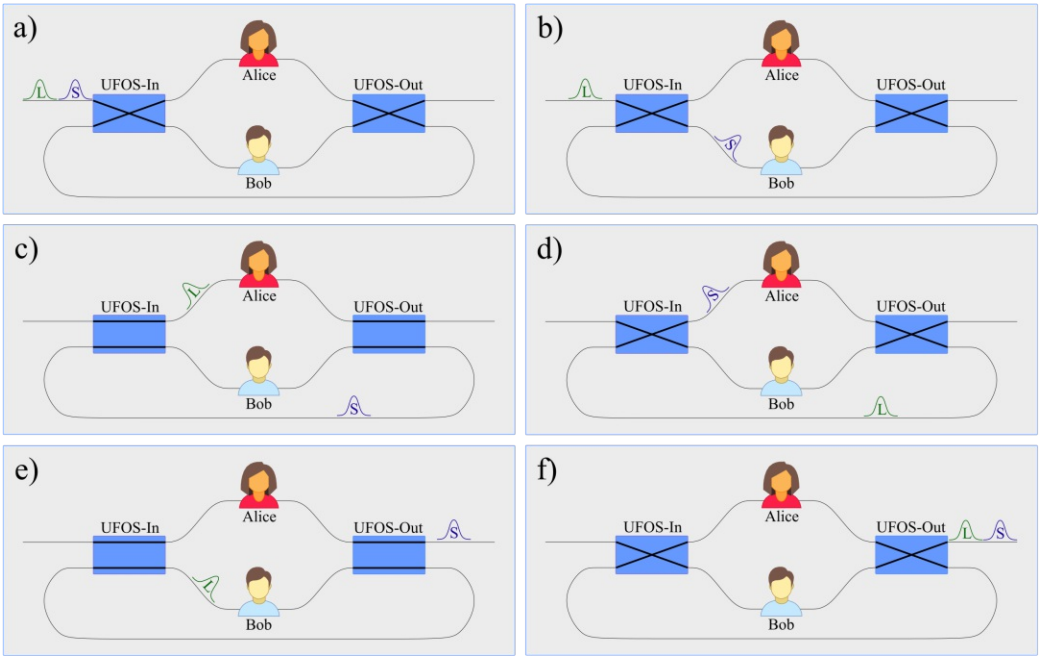

Figure 3.3: In this figure, the path taken by the individual time-bins is illustrated. Panel **a)** shows the states $|S\rangle$ and $|L\rangle$ approaching the quantum SWITCH. In panel **b)** both UFOSs (UFOS-In, -Out) are in 'cross' so that $|S\rangle$ takes the path to Bob's laboratory. In **c)** the UFOSs are in 'bar' and $|L\rangle$ propagates now first to Alice's laboratory, while $|S\rangle$ passes UFOS-Out in 'bar' and therefore loops back to UFOS-In. Next, in panel **d)** $|S\rangle$ takes this time the path to Alice, while $|L\rangle$ loops back to UFOS-In. In **e)**, $|S\rangle$ already leaves the quantum SWITCH and $|L\rangle$ enters Bob's laboratory. Finally, in **f)** both time-bins passed the SWITCH so that the photon is now in state $|S\rangle_{\mathrm{C}}\, AB\, |\Psi\rangle_{\mathrm{T}} + |L\rangle_{\mathrm{C}}\, BA\, |\Psi\rangle_{\mathrm{T}}$.

After the 2-switch operation is applied to the photon, the two time-bins in states $|S\rangle\, AB\, |\Psi\rangle$ and $|L\rangle\, BA\, |\Psi\rangle$ pass another fiber optical circulator back to UFOS-MZI, which directs them along the fiber loop in clockwise direction. Additionally, this circulator ensures that no light accidentally propagates the quantum SWITCH in counter-clockwise direction. The combination of UFOS-MZI and the FDC, which initially generated the time-bins appears now as Mach-Zehnder-Interferometer (MZI) [21], where the bins can be recombined and hence, interfere. To do so, $|S\rangle$ passes the optical switch in its 'cross' state and propagates along the long path. With the feed-forward protocol the UFOS can go into its 'bar' state and hence, $|L\rangle$ takes the short path of the MZI. One of the FDC outputs serves directly as an output for the MZI, while the other one connects to the initial optical circulator. Now, the

Die approbierte gedruckte Originalversion dieser Diplomarbeit ist an der TU Wien Bibliothek verfügbar
The approved original version of this thesis is available in print at TU Wien Bibliothek.
TU Bibliothek Your knowledge hub WIEN

light takes the third output of the circulator and therefore acts as the second output of the MZI. Since in total both time-bins $|S\rangle$ and $|L\rangle$ have seen the same sections of fiber and therefore expirenced the same changes in phase, the MZI is passively phase stable. Finally, to achieve a high interference visibility we can match the polarization of the time-bins with a fiber paddle polarization controller inside the MZI.

Die approbierte gedruckte Originalversion dieser Diplomarbeit ist an der TU Wien Bibliothek verfügbar
The approved original version of this thesis is available in print at TU Wien Bibliothek.
TU WIEN Bibliothek Your knowledge hub

Die approbierte gedruckte Originalversion dieser Diplomarbeit ist an der TU Wien Bibliothek verfügbar
The approved original version of this thesis is available in print at TU Wien Bibliothek.

Chapter 4

Results

4.1 Photonic Maxwell's Demon

In this chapter the experimental results of the photonic Maxwell's Demon experiment are presented. In the first section the characteristic measurements for the investigated input states are presented, e.g the second order correlation function or the Hong-Ou-Mandel dip. In the second section, the observed 'power of the MD' is presented.

4.1.1 Characterization of the Photon States

First, we present characteristic measurements for the respective input states with which the 'power of the MD' was probed. As is explained in Ch. 3.1, we generated uncorrelated thermal states by scattering classical light on a spinning ground glass. To verify the thermal nature of these states, we measured the second order correlation function $g^{(2)}(\tau)$ by sending one of the states on a balanced beamsplitter while monitoring its output ports. As mentioned in Ch. 2.2.2 for thermal light characteristically the $g^{(2)}(0) = 2$. The measured correlation function is presented in Fig. 4.1 a). From fitting a gaussian thermal beam, $g^{(2)}(\tau) = 1 + e^{-\pi(\tau/\tau_c)^2}$, we obtained a $g^{(2)}(0) \approx 1.95$ and extracted a coherence time of $\tau_c = 5.42\mu$s.

We also probed the MD with a split thermal state. Generating such a state is as easy as splitting a single thermal beam, on a balanced beamsplitter. In order to confirm that the thermal nature of this state is still present, we again measured the $g^{(2)}(\tau)$. The obtained correlation function is presented in Fig. 4.1 b) with a $g^{(2)}(0)$ close to 2.

The correlated thermal states are generated by SPDC. We estimated the photons coherence time via HOM-interference and obtained $\tau_c \approx 2$ ps. The measured HOM-dip is shown in Fig. 4.1 c). Since the coherence time is much smaller than the resolution of our time tagging module (156 ps) and the timing jitter ($\approx$ 200 ps) of the detectors, we were unable to measure a $g^{(2)}(\tau)$ and hence, verify the thermal nature of the states. However, it is well known, that for SPDC photon sources the idler (signal) beam is from

Die approbierte gedruckte Originalversion dieser Diplomarbeit ist an der TU Wien Bibliothek verfügbar
The approved original version of this thesis is available in print at TU Wien Bibliothek.
TU Bibliothek Your knowledge hub WIEN

thermal nature when the signal (idler) beam is traced out [33].

As just mentioned, we perform HOM-interference in order to prepare the anti-correlated NOON-state from the two SPDC photons. In order to determine the quality of the HOM interference, we scanned the relative path difference of the photons to measure the visibility $v^2 = 0.87 \pm 0.02$ of the HOM-dip (see Fig. 4.1 c)).

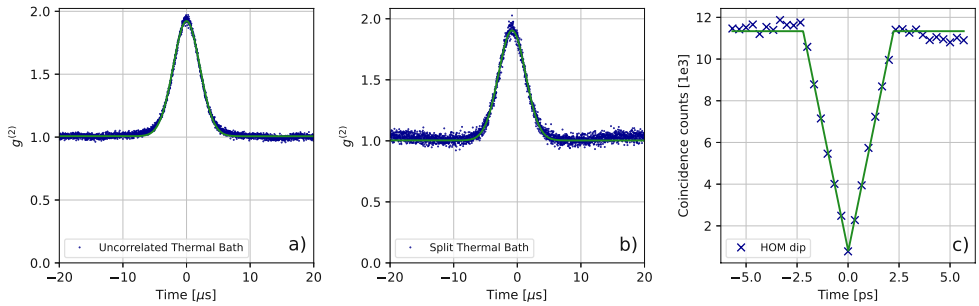

Figure 4.1: This figure shows the characteristic measurements of the different input states. In **a)**, the $g^{(2)}(\tau)$ measurement of the thermal beam can be seen, while **b)** shows the corresponding measurement for one mode of the split thermal state. Both exhibit a $g^{(2)}(\tau)$ very close to 2. **c)** shows the HOM-dip (with visibility $v^2 = 0.87 \pm 0.02$) from interfering the signal and idler photon from the SPDC source.

4.1.2 The 'Power' of the photonic Maxwell's Demon

In the following, the experimental results for 'the power of MD' are presented. We evaluate the figure of merit $\Delta N/N$ and $\Delta N/C$ (see Ch. 2.3.2) by measuring the photon number imbalance ΔN induced by MD. But first, the measurement procedure implemented for the different input states is explained. Clearly, this quantity is highly sensitive to an input photon number imbalance as well as to non-equal losses in modes A and B. Hence we had to come up with a technique to take this into account. To do so we first fix the UFOS to the 'cross' state and balance the count rates N_A and N_B, measuring at detectors D_A and D_B so that $\Delta N_{\text{cross}} = N_A - N_B \approx 0$. Second, we determine the intrinsic imbalance of the setup. Therefore, we fix the UFOS to the 'bar' state and measure the photon number imbalance $\Delta N_{\text{bar}} = N_A - N_B$ between detectors D_A and D_B. This quantity represents the maximum imbalance that the demon can experimentally create without using the information obtained about the thermal states. Next, we turn on the feed-forward (FF) mechanism so that the demon is active. This results in a photon number

Die approbierte gedruckte Originalversion dieser Diplomarbeit ist an der TU Wien Bibliothek verfügbar
The approved original version of this thesis is available in print at TU Wien Bibliothek.
TU Bibliothek Your knowledge hub WIEN

imbalance between detectors D_A and D_B of $\Delta N_{\mathrm{FF}} = N_A - N_B$. From that, the unnormalized 'power of MD' is defined as

$$\Delta N := \Delta N_{\mathrm{FF}} - \Delta N_{\mathrm{bar}} \,. \tag{4.1}$$

Finally, to obtain the figure of merit we have to normalize ΔN by either the singles rate or the coincidence rate. For normalizing by the singles counts, we measure the number of photons detected by D_A and D_B for the different reflectivity settings of the TDC and divide each rate by $(1 - R^2)$, where R is the reflection amplitude. This gives us the incoming singles rate at the TDC's. Finally we average these values over mode A and B, which we define as the incoming singles rate N. To obtain the incoming coincidence rate, the calculations is similar. Since we were limited in our coincidece logic, we only measured the coincidence rates between detectors D_A and Dem_A (C_{D_A,Dem_A}) detectors D_A and Dem_B (C_{D_A,Dem_B}) when the TDS's reflectivity is set to 50%. This allows us to calculate the input coincidence rate for both correlated and anti-correlated thermal states.

This measurement procedure was applied to all four input states and from the measurement outcomes we evaluated the 'power of MD' according to the models constructed in Ch. 2.3.2 for different reflectivity setting going from 0% to 50% of the TDC's. In all measurements, the switching pulse of the function generator, which enables the demon to swap modes, was set to 2.5 μs. For the measurement of the 'demons power' in the low photon regime for uncorrelated thermal states, we set the average photon number at D_A and D_B to 27800 ± 500. We fit the data with the corresponding model from Ch. 2.3.2, which contains only one fitting parameter. For uncorrelated thermal states this is the average photon number per mode $\bar{n}$. From the incoming photon rate and the light's coherence time of 5.42 μs we would expect $\bar{n} = 0.151 \pm 0.002$ Hz. However, since the switching time of the feed-forward logic is smaller than the photons coherence time it is likely, that some bunched events are not swapped between the modes correctly and thus the 'demons power' is reduced. Hence, we find a much better fit for $\bar{n} = 0.05$. The data is presented in Fig. 4.2 a) and b). Since the waveform generator can not respond during the time a trigger event is being processed, increasing the length of the switching pulse does not lead to an improve in the 'demons power'.

We performed the same measurement procedure for split thermal light. Here we balance the input count rates to 293000±3000 Hz, which corresponds to a $\bar{n} \approx 0.7$. The experimentally measured $\Delta N/N$ is shown in Fig. 4.2 a). The non-zero effect of the demon is very likely due to imbalanced losses in the setup. However, since the count rate of the incident photons is much

Die approbierte gedruckte Originalversion dieser Diplomarbeit ist an der TU Wien Bibliothek verfügbar
The approved original version of this thesis is available in print at TU Wien Bibliothek.
TU Bibliothek Your knowledge hub WIEN

higher than in the uncorrelated case, one can still say that the demon effect practically vanishes.

For correlated thermal states as input, we balance the incoming count rate to 168000 ± 1000 Hz. Due to the small coherence time of 2 ps, this results in an average photon number per mode of $\bar{n} \approx 10^{-7}$. We normalized the recorded data and fitted it with our theoretical model, which again has only one free parameter ϵ^2 (coupling efficiency). We estimated $\epsilon^2 = 0.14$, from separate measurements. The result is shown in Fig. 4.2 a). As mentioned in Ch. 2.3.2 we also want to normalize this data by the incoming coincidence rate C. This makes the figure of merit $\Delta N/C$ independent from the coupling efficiency and therefore, the model contains not a single fitting parameter anymore. The data and the very good prediction by the model are shown in Fig. 4.2 b).

Finally we present the results for anti-correlated thermal states as an input. Here, the singles rates are balanced to 141000 ± 3000 Hz and hence, $\bar{n} \approx 10^{-7}$. Again, the measurement procedure stays the same and the results for $\Delta N/N$ are presented in Fig. 4.2 a). For the theoretical model we use the measured HOM-visibility $v^2 = 0.87$ and a coupling efficiency of again $\epsilon^2 = 0.14$. When normalizing the 'demons power' with the incoming coincidence rate, the coupling efficiency drops again out. Again, our data is in very good agreement with the theoretical prediction and is shown in Fig. 4.2 b).

Die approbierte gedruckte Originalversion dieser Diplomarbeit ist an der TU Wien Bibliothek verfügbar
The approved original version of this thesis is available in print at TU Wien Bibliothek.
TU Bibliothek Your knowledge hub WIEN

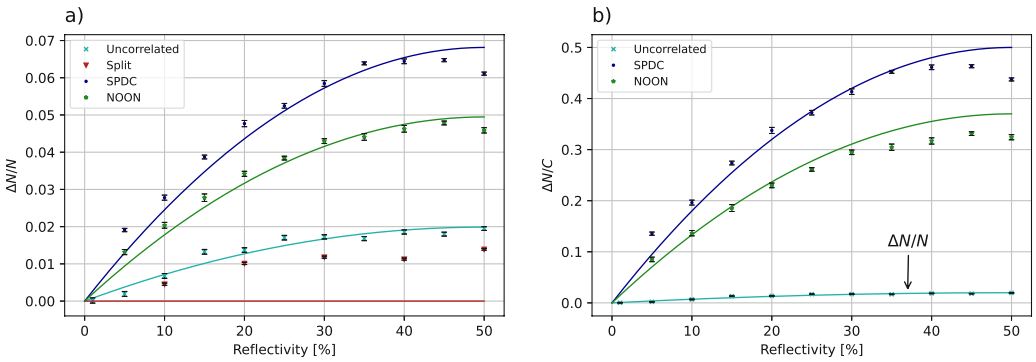

Figure 4.2: This figure presents the figure of merit for the demons 'power'. **a)** shows the generated photon number imbalance normalized by the incoming singles rate N, while **b)** shows the obtained data normalized by the incoming coincidence rate C. The solid lines represent the theoretical models: uncorrelated thermal state with $\bar{n} = 0.05$ (turqoise), split thermal state with $\Delta N/N = 0$ (red), correlated thermal state with $\epsilon^2 = 0.14$ (green) and anti-correlated thermal state with $\epsilon^2 = 0.14$ and $v^2 = 0.87$ (blue). The error bars represent standard deviations of the measurement sets.

Fig. 4.2 shows the excellent agreement between the theoretical predictions and our experimental data. The measured data deviate slightly from theory only at higher reflectivity values. This is because our simplified theoretical model does not take into account the detection efficiency of the demon. This property has already been shown by the theory developed in [8] that changes in the relative detection efficiency between Dem_A and Dem_B can shift the dependency on ΔN on the reflectivity.

4.2 Quantum SWITCH

In this section the experimental results from the measurements taken on the quantum SWITCH are presented.

4.2.1 The 2-SWITCH Operation with Pauli-Operators

As a first step of investigating this new architecture of the quantum SWITCH we wanted to reproduce the results from the first experimental realization of the SWITCH by Procopio *et al* [4]. In this paper they realized a quantum SWITCH in an optical bulk setup with the control qubit encoded in the path

Die approbierte gedruckte Originalversion dieser Diplomarbeit ist an der TU Wien Bibliothek verfügbar
The approved original version of this thesis is available in print at TU Wien Bibliothek.
TU Bibliothek Your knowledge hub WIEN

degree of freedom of the photon. They demonstrated its ability of superimposing quantum gate orders by solving the computational problem introduced in Ch. 2.4.1, where the goal is to decide whether two unitary gates commute or anti-commute. As mentioned the quantum SWITCH investigated in this work is based on UFOS's, which route the photon through fiber to the two polarization gates depending on the state of the time-bin encoded control qubit. Since optical fibers are strongly birefringent it is not straight forward to ensure that the photon only experiences the transformations on its polarization state, that are carried out by Alice and Bob. In general, the fibers, which are guiding the photon between the gates, perform arbitrary unitary operations on the photons polarization. This makes it impossible to determine the commutation relation between the two unitary gates. Hence, it is essential to set these arbitrary transformations equal to the identity transformation. This turned out to be quite challenging. However, we developed a technique to achieve the required transformation, which is presented in the appendices.

In order to demonstrate the computational task, we chose the unitary gates implemented by Alice and Bob to be the Pauli operators

$$\hat{\sigma}_I \equiv \begin{pmatrix} 1 & 0 \\ 0 & 1 \end{pmatrix}, \hat{\sigma}_X \equiv \begin{pmatrix} 0 & 1 \\ 1 & 0 \end{pmatrix}, \hat{\sigma}_Y \equiv \begin{pmatrix} 0 & -i \\ i & 0 \end{pmatrix}, \hat{\sigma}_Z \equiv \begin{pmatrix} 1 & 0 \\ 0 & -1 \end{pmatrix}, \tag{4.2}$$

which have the well known commutation relation $[\hat{\sigma}_i, \hat{\sigma}_j] = 2i\epsilon_{ijk}\hat{\sigma}_k$ and anti-commutation relation $\{\hat{\sigma}_i, \hat{\sigma}_j\} = 2\delta_i j \mathbb{1}_{2x2}$ [24]. Here, ϵ_{ijk} is the Levi-Civita symbol and $\delta_i j$ is the Kronecker delta. In words, each operator commutes only with itself or identity and anti-commutes for all $\hat{\sigma}_i \neq \hat{\sigma}_j$ with $i, j \in \{X, Y, Z\}$. From Eq. 2.41 we can see that, depending on which statement is true, the photon always leaves one of the ports of the beam splitter shown in Fig. 3.2. We defined the bright port in case of two commuting operators as 'port 0' and the one for anti-commuting operators as 'port 1'. In order to obtain the corresponding probabilities for both statements, we measured coincidences between the heralding photon and the signal photon after passing through the experiment. The coincidence window was set to 5 ns while the detection events were integrated over 10 s. The visibility of the interferometer for interfering the time-bins was $v^2 = 0.97$. Fig. 4.3 shows the experimental results from this measurement.

Die approbierte gedruckte Originalversion dieser Diplomarbeit ist an der TU Wien Bibliothek verfügbar
The approved original version of this thesis is available in print at TU Wien Bibliothek.
TU Bibliothek Your knowledge hub WIEN

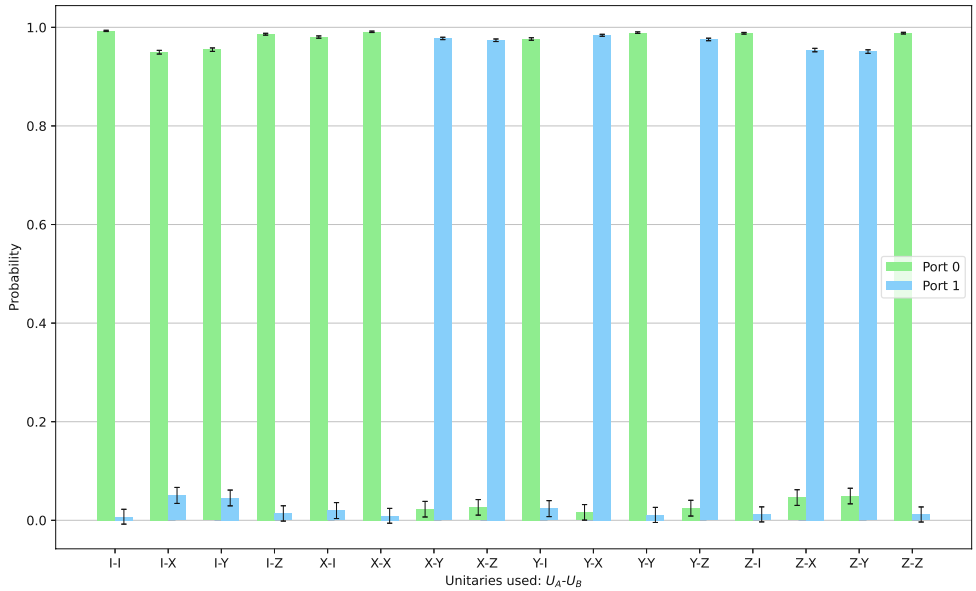

Figure 4.3: This figure shows the experimentally estimated probabilities that two arbitrary unitary gates U_A and U_B either commute or anti-commute. The green bars represent the probability, that the photon leaves port 0 (commuting), while the blue bars represent the probability for the photon to exit port 1 (anti-commuting). The x-axis labels which gates U_A and U_B Alice and Bob have implemented in the SWITCH (They labels imply $I = \sigma_I$, $X = \sigma_X$, $Y = \sigma_Y$, $Z = \sigma_Z$).

The experimentally measured probabilities are in very good agreement with the theoretical commutation- and anti-commutation relations. We defined a success probability for the photon leaving the correct port as the average probability that the photon leaves port 0 for commuting gates and and port 1 for anti-commuting gates. Mathematically this is expressed as

$$p_{\text{succ}} = \frac{1}{2}(\bar{p}(0|C) + \bar{p}(1|A)) \tag{4.3}$$

for what we obtained and experimentally estimated value of $p_{\text{succ}} = 0.974 \pm 0.007$.

4.2.2 Witnessing Causal Non-Separability

As a second step we want to verify the indefinite causal order of the gates applied to a target qubit in the quantum SWITCH. Therefore we measure

Die approbierte gedruckte Originalversion dieser Diplomarbeit ist an der TU Wien Bibliothek verfügbar
The approved original version of this thesis is available in print at TU Wien Bibliothek.
TU Bibliothek Your knowledge hub WIEN

the mathematical object introduced in Ch. 2.4.4 called a 'causal witness'. This has first been done by Rubino *et al* [5] on a very similar SWITCH setup to the one from Ref. [4]. The significant difference in Rubino's experimental setup was that they implemented a measurement/re-preparation channel (see Ch. 2.4.3) for one of the two parties, Alice and Bob, while the other had only access to unitary operations. The presence of these more complex channels increases the theoretically measurable value of the causal witness.

In this work we verified the causal non-separability of the gate order in our quantum SWITCH by measuring a causal witness with two different kind of gates implemented by Alice and Bob. First we provided the two parties access to only unitary operations on the target qubit. As was explained in Ch. 2.4.3 these gates can be realized by sandwiching a $\lambda/2$-waveplate with two $\lambda/4$-waveplates. The witness, which we measured with two unitary gates U_A and U_B can mathematically expressed as

$$\mathrm{Tr}\{\hat{S}W\}_{U_A,U_B} = \sum_{x=1}^{10}\sum_{y=1}^{10}\sum_{d=1}^{2}\alpha_{d,x,y,z}p(d|x,y,z=|H\rangle)\,. \tag{4.4}$$

Since we probed the SWITCH only with one input state, $|H\rangle$, we do not need to sum over z in Eq. 4.4. The same applies for a and b (see Eq. 2.55), because the unitary gates do not have a measurement outcome. To find the best possible witness $\hat{S}$ for this configuration, we use 'Matlab'-code from a colleague, Mateus Araújo, which takes the ideal process matrix of the SWITCH and a set of available operations as an input and returns the 'strongest' possible witness to implement in the measurement. Alice and Bob had access to 10 different unitary operators, which are considered by the variables x and y. Finally we measure coincidences at the two outputs of the beamsplitter and hence, $d \in \{1,2\}$ corresponding to projecting the control qubit onto $|+\rangle$ or $|-\rangle$. The probability in Eq. 4.4 is defined as $p(d|x,y,z=|H\rangle) = \mathrm{Tr}\{(\rho^{\mathrm{in}}_{z=|H\rangle} \otimes U^{\mathrm{A}}_x \otimes U^{\mathrm{B}}_y \otimes D^{\mathrm{out}}_d)W_{SWITCH}\}$. Fig. 4.4 a) and c) show some of the measured probabilities $p(d|x,y,z=|H\rangle)$ for the photon leaving either port 0 or 1 respectively, while Fig. 4.4 b) (Port 0) and d) (Port 1) graphically illustrate the individual terms of Eq. 4.4. Again, the coincidence window was chosen to span 5 ns with an integration time of 10 s and the interferometric visibility was $v^2 = 0.97$.

Die approbierte gedruckte Originalversion dieser Diplomarbeit ist an der TU Wien Bibliothek verfügbar
The approved original version of this thesis is available in print at TU Wien Bibliothek.
TU Bibliothek Your knowledge hub WIEN

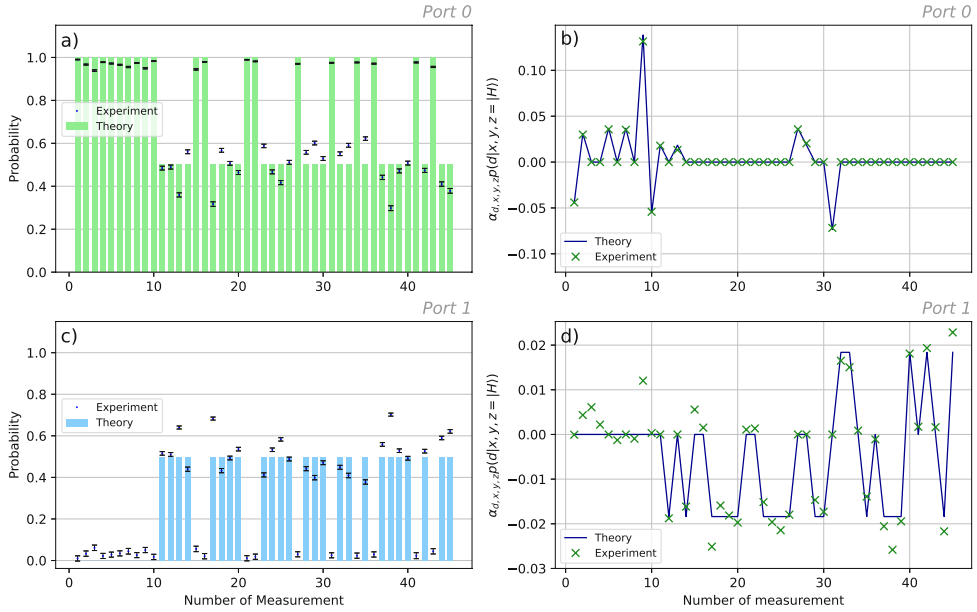

Figure 4.4: This figure shows the experimental results from the performed causal tomography for the case, that Alice and Bob have only access to unitary operations. **a)** and **c)** show the estimated probabilities that the photon exits port 0 or 1 respectively. In both graphs the bars represent the theoretical predictions, while the dot markers with error bars show the experimentally measured values. Panel **b)** and **d)** graphically illustrate the corresponding terms in Eq. 4.4 given by the probabilities times the weight $\alpha_{d,x,y,z}$. Here, the blue line gives the theoretical prediction, while the 'x' markers show the experimentally obtained weighted probabilities. Note that the solid line for the theoretical values has no physical meaning, but is a visual aid for displaying the data.

The measurement from Fig. 4.4 required 74 different experimental settings with each two different measurement outcomes. Hence, the sum in Eq. 4.4 has 148 terms. Note that, out of demonstrative reasons, we only present here the first 45 settings. Out of this we evaluate the causal non-separability of the quantum SWITCH in this configuration to be

$$\mathrm{Tr}\{\hat{S}W\}_{U_A,U_B} = -0.138 \pm 0.006\,. \tag{4.5}$$

This result is very close to the theoretical obtainable value of -0.151. The main reasons for the disagreement between the theoretical prediction and the experimental result are miss calibrations of the motorized waveplates and imperfect fiber polarization compensation in the SWITCH.

Die approbierte gedruckte Originalversion dieser Diplomarbeit ist an der TU Wien Bibliothek verfügbar
The approved original version of this thesis is available in print at TU Wien Bibliothek.
TU Bibliothek Your knowledge hub WIEN

Next, we measured a causal witness on the quantum SWITCH when both parties, Alice and Bob, have access to measurement/re-prepare channels M_A and M_B. As already mentioned above, implementing these type of gates, allows us to acquire more information about the system and hence, a 'stronger' witness can be accessed. For this measurement, we probed the SWITCH with the target qubit in $|V\rangle$ as an input. Now, both parties can learn something about the incoming quantum state and therefore, their local operations have outcomes a and b. To obtain the experimental probabilities we measured the control again in the diagonal basis by monitoring both outputs of the beamsplitter. Hence, the causal witness for this configuration can be expressed as

$$\mathrm{Tr}\{\hat{S}W\}_{M_A,M_B} = \sum_{x=1}^{24}\sum_{y=1}^{24}\sum_{d=1}^{2} \alpha_{a,b,d,x,y,z} p(a,b,d|x,y,z=|V\rangle)\,. \tag{4.6}$$

Since we only project on the horizontal polarization state $|H\rangle$, we still don't have to sum over the parameters a and b. The probability in Eq.4.6 is defined as $p(a,b,d|x,y,z = |V\rangle) = \mathrm{Tr}\{(\rho^{\mathrm{in}}_{z=|V\rangle} \otimes M^{\mathrm{A}}_{a,x} \otimes M^{\mathrm{B}}_{b,y} \otimes D^{\mathrm{out}}_{d})W_{SWITCH}\}$. Fig. 4.5 a) and c) show some of the experimentally estimated probabilities and Fig. 4.5 b) and d) the graphically illustrated terms of Eq. 4.6. The visibility of the interferometer was $v^2 = 0.97$ and the coincidence window was chosen to be 5 ns with an integration time of 10 s.

Die approbierte gedruckte Originalversion dieser Diplomarbeit ist an der TU Wien Bibliothek verfügbar
The approved original version of this thesis is available in print at TU Wien Bibliothek.
TU Bibliothek Your knowledge hub WIEN

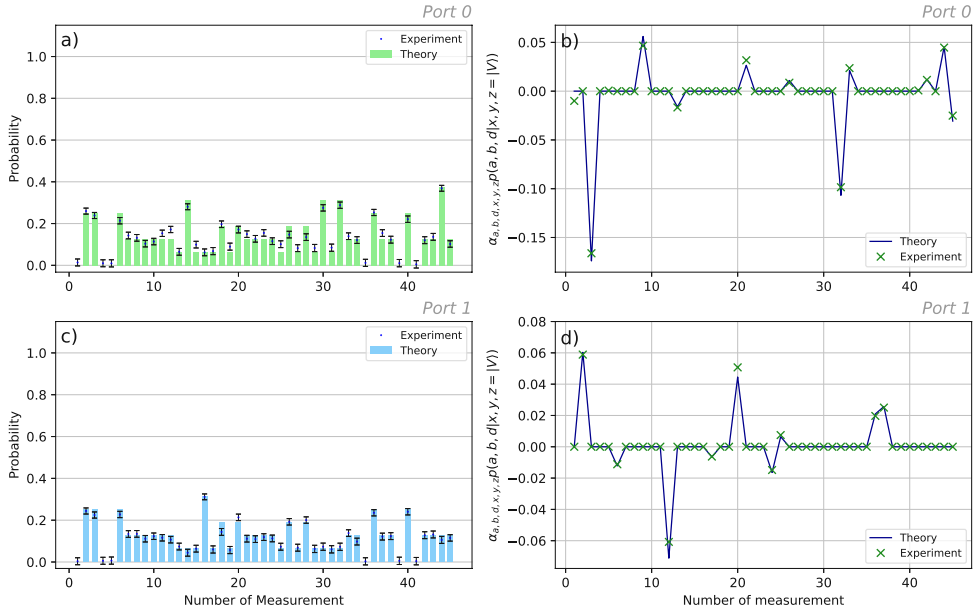

Figure 4.5: This figure shows the experimental results from the performed causal tomography for the case, that both, Alice and Bob, have access to measurement/re-preparation channels. **a)** and **c)** show the estimated probabilities that the photon exits port 0 or 1 respectively. Again the bars represent the theoretical predictions, while the dot markers show the experimentally measured values. Panel **b)** and **d)** graphically illustrate the corresponding terms in Eq. 4.6. Again, the blue line gives the theoretical prediction, while the 'x' markers show the experimentally obtained weighted probabilities. Also here the solid line representing the theoretical values has no physical meaning, but is a visual aid for presenting the data.

For the measurement from Fig. 4.5 we implemented 408 experimental settings, together with the two measured output ports of the beamsplitter this results in 816 terms in Eq. 4.6. Again, we only show the first 45 measurements for the sake of clarity. We calculate the causal non-separability from the experimental data to be

$$\mathrm{Tr}\{\hat{S}W\}_{M_A,M_B} = -0.193 \pm 0.07\,. \tag{4.7}$$

Here, the maximum theoretically obtainable value is -0.341. Again, as for the unitary gates, the main sources for errors are miss settings of waveplates and the fiber polarization compensation in the SWITCH. Additionally, the simulations showed, that the expected probabilities are also extremely sensitive to miss settings of the polarizer in each gate. Nevertheless, we could clearly verify the indefinite causal order of the quantum gates.

Die approbierte gedruckte Originalversion dieser Diplomarbeit ist an der TU Wien Bibliothek verfügbar
The approved original version of this thesis is available in print at TU Wien Bibliothek.
TU Bibliothek Your knowledge hub WIEN

4.2.3 Process Tomography

In earlier experimental work only the causal non-separability of the quantum SWITCH was verified, the underlying process, however, remained undefined [5][4]. In order to undertake first the full characterization of the quantum SWITCH, we performed quantum process tomography on the device. To do so we probe the SWITCH with two different input states, $|H\rangle$ and $|D\rangle$, while Alice and Bob perform different measurement/re-preparation operations on the target qubit. Finally we measure the state of the control qubit in the computational and diagonal basis. In order to determine the process matrix from the experimentally estimated probability list p_{exp} for the certain outcomes, we must first calculate the theoretical probability values according to Eq. 2.58, where W is the ideal process matrix of the quantum SWITCH. Together with these ideal probabilities p_{id} and the knowledge about the operations applied by Alice and Bob, Eq. 2.58 results in a list of constraints for the desired process matrix. Together with the constraints for a physical process matrix (see Eq. 2.59a-c), a semi-definite programming algorithm solves a minimization problem to find the best fitting and physical process matrix to our experimentally obtained probabilities. In fact, we are minimizing the expression $\sqrt{\sum_i (p^i_{exp} - \text{Tr}^i\{W_{\text{exp}}(\rho^{\text{in}}_z \otimes M^{\text{A}}_{a,x} \otimes M^{\text{B}}_{b,y} \otimes D^{\text{out}}_d)\})^2}$, where the trace corresponds to Eq. 2.58 and results in the probability for a certain outcome. However, since W_{exp} is the only unknown parameter, minimizing this expression leads to the best suitable process matrix W_{exp} for our device. The real and complex part of the ideal and experimentally estimated process matrix of the quantum SWITCH is graphically illustrated in Fig. 4.6 by a three-dimensional bar chart.

To estimate, how close our measurement results are to the theoretical prediction, we calculate the fidelity between the two process matrices according to $F(\rho, \sigma) = \text{Tr}\{\sqrt{\sqrt{\rho}\sigma\sqrt{\rho}}\}$ [24]. Since the process matrix is a very similar object to the density operator, with exception of $\text{Tr}\{W\} \neq 1$, we first normalize the process matrices according to $\tilde{W} = W/\,\text{Tr}\{W\}$ before we plug it into the formula for the fidelity. Doing so we can calculate a fidelity of $F(\tilde{W}_{\text{id}}, \tilde{W}_{\text{exp}}) = 0.753$, where $\tilde{W}_{\text{id}}$ ($\tilde{W}_{\text{exp}}$) is the ideal (experimental) process matrix of the SWITCH. Since both Alice and Bob perform projective measurements and additional we perform quantum state tomography on the control qubit at the output, the process tomography performed on the switch is equivalent to a 6-qubit tomography. Considering that, our result is in excellent agreement with the theoretical prediction. In addition, we extracted the causal non-separability directly out of the measured process matrix. To do so, we use the same 'Matlab'-code as to find a witness for the causal tomography, but this time the code gets a set of possible operations and the experimen-

Die approbierte gedruckte Originalversion dieser Diplomarbeit ist an der TU Wien Bibliothek verfügbar
The approved original version of this thesis is available in print at TU Wien Bibliothek.
TU Bibliothek Your knowledge hub WIEN

tally estimated process matrix of the SWITCH as an input. With this we could calculate the causal non-separability to $\mathrm{Tr}\{\hat{S}W_{\mathrm{exp}}\}_{M_A,M_B} = -0.183$. With the same set of operations and the ideal process matrix the theoretical limit is -0.549. At the moment we believe that the main reason for the discrepancy between the experimentally estimated value and the theoretical limit is a combination of an non-ideal interference visibility, errors in the polarization compensation of the SWITCH's fibers and miss-calibration of the motorized waveplates. We are currently trying to check this rationale by simulating these sources of error. However, this clearly verifies that the gates in our new architecture for the quantum SWITCH exhibit an indefinite causal order.

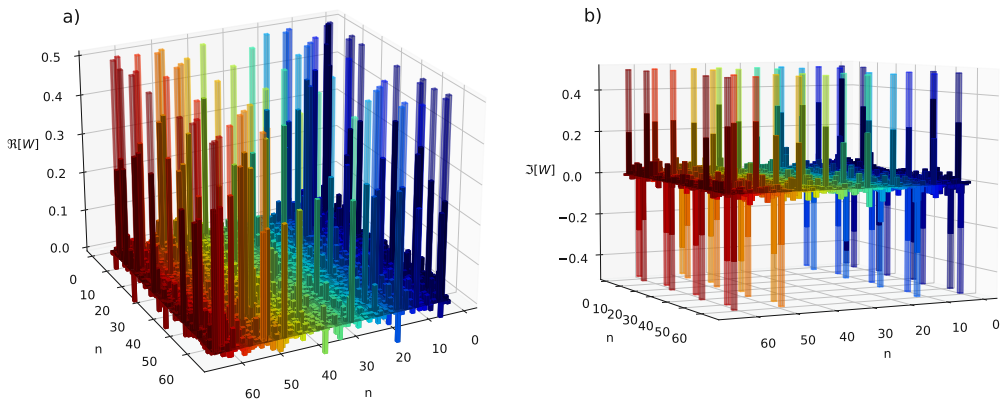

Figure 4.6: This figure represents the ideal and experimentally obtained process matrix of the quantum SWITCH. Panel **a)** illustrates the real part of the matrix, while **b)** shows the imaginary part. For demonstrative reasons, the x-scale has been color-coded as it serves as a visual aid to identify which matrix elements are represented by the individual bars. To compare the experimental data to the ideal values of the matrix elements, the ideal process matrix is visualized in slightly transparent bars, while the non-transparent bars represent the measured values.

Die approbierte gedruckte Originalversion dieser Diplomarbeit ist an der TU Wien Bibliothek verfügbar
The approved original version of this thesis is available in print at TU Wien Bibliothek.
TU Bibliothek Your knowledge hub WIEN

Die approbierte gedruckte Originalversion dieser Diplomarbeit ist an der TU Wien Bibliothek verfügbar
The approved original version of this thesis is available in print at TU Wien Bibliothek.

Chapter 5

Conclusion & Outlook

5.1 Photonic Maxwell's Demon

To summarize the photonic Maxwell's Demon experiment of this work, we successfully implemented the thought experiment in the photonic domain. In comparison to the earlier proposal from [7] our demon is capable of actually swapping particles between modes. Moreover we have experimentally proven the enhancement of the 'demons power' in the low photon regime when different correlated thermal states are used as inputs. Therefore a natural continuation of this project would be to test the 'demons power' with higher average photon numbers per mode $\bar{n}$. Since the anti-correlated states act similar to the thermal correlations, we would expect them to perform the best in the higher photon number regime. This would require to generate N00N-states with $N > 2$ and likely a SPDC photon pair source with a pulsed laser for pumping in order to raise the probability for multi photon-emission events.

5.2 Fiber-Based Quantum SWITCH

In summary, we presented a new passively-stable fiber based architecture for the quantum SWITCH based on UFOS. We implemented a new way to coherently control the gates order by using time-bin encoded qubits. We have shown that our implementation, like the first experimental realization of the SWITCH [4], is capable of determining whether any two unitary gates either commute or anti-commute. Further, we have verified the indefinite causal order of the gates by performing causal tomography. Also we have experimentally determined the process matrix of the quantum SWITCH and estimated its fidelity to the ideal process matrix for the first time.

Since our architecture can readily be scaled to more parties, it would be logical approach to so. In order to generate all gate permutations, this includes the expansion of the here proposed passively-stable interferometer for creating and interfering time-bins to operate with higher dimensional qudits.

Die approbierte gedruckte Originalversion dieser Diplomarbeit ist an der TU Wien Bibliothek verfügbar
The approved original version of this thesis is available in print at TU Wien Bibliothek.
TU Bibliothek Your knowledge hub WIEN

To the best of our knowledge, no causal witness has yet been measured on a quantum SWITCH with more than two quantum gates.

Die approbierte gedruckte Originalversion dieser Diplomarbeit ist an der TU Wien Bibliothek verfügbar
The approved original version of this thesis is available in print at TU Wien Bibliothek.
TU WIEN Bibliothek Your knowledge hub

Appendices

Die approbierte gedruckte Originalversion dieser Diplomarbeit ist an der TU Wien Bibliothek verfügbar
The approved original version of this thesis is available in print at TU Wien Bibliothek.

Die approbierte gedruckte Originalversion dieser Diplomarbeit ist an der TU Wien Bibliothek verfügbar
The approved original version of this thesis is available in print at TU Wien Bibliothek.

Appendix A

Fiber Polarization Compensation

One of the major issues in the quantum SWITCH experiment was to deal with undesired arbitrary unitary transformations on the target qubit induced by the birefringence of the the optical fibers. As mentioned above, all measurements were very sensitive to these undesirable changes in the photon polarization. Therefore, we had to come up with a compensation technique for setting these unitary transformations caused by the the fiber to identity operators. Hence, the fiber has no effect on the photon polarization so that gate A can directly act after gate B or vice versa. The most successful approach for this was to use classical light as input and then measure the polarization of the light with a polarimeter (Thor Labs PAX1000IR2/M) at different points in the SWITCH, e.g. we route the light directly to gate A and measure the polarization after the fiber link. As it can be seen in Fig. 3.2, each fiber connection is equipped with fiber paddle polarization controllers. In order to prepare a true identity operator it is essential that the fiber performs the identity operation in two different bases. Hence, we prepared at the u-bench before the SWITCH in alternating order the input states $|H\rangle$ and $|D\rangle$, while adjusting the fiber paddles. This process converges to a point, where each state is mapped to it self and the fiber performs a true identity operation. When applying this procedure to the fibers, which lead back to the initial UFOS we place an additional polarizer in the gate passed first and adjust the paddles right after the same gate, eg. when we want to compensate the fiber, that runs from gate A to gate B, we place the polarizer in A, set it to the corresponding state, which we want to map and measure the polarization in gate B. Moreover, it turned out, that the compensation is extremely sensitive to the wavelength of the light. Hence, it was essential, that the wavelength of the classical light matched exactly the single-photon wavelength.

Die approbierte gedruckte Originalversion dieser Diplomarbeit ist an der TU Wien Bibliothek verfügbar
The approved original version of this thesis is available in print at TU Wien Bibliothek.
TU Bibliothek Your knowledge hub WIEN

Die approbierte gedruckte Originalversion dieser Diplomarbeit ist an der TU Wien Bibliothek verfügbar
The approved original version of this thesis is available in print at TU Wien Bibliothek.

Acknowledgments

While developing this thesis I was supported by numerous people whose contribution was essential for me and the progress of this work. Therefore it would be an outrage not to express my deepest thanks to these people.

First of all a big thank you goes to Lee Rozema, who did a great job in supervising me in this project. No matter which problems I was facing in the Lab, the discussions with him always leaded me one step forward.

I would also like to thank Guilherme L. Zanin, who was my partner in the Maxwell's Demon experiment. He was the one who started this project, but always treated me as an equal, while we were working on the project together.

My next thanks goes to Michele Spagnolo, who did an amazing contribution with the work on the SPDC source.

Moreover, I would also like to thank Robert 'Bob' Peterson for helping me with any electronics problems I had to solve.

Another thank you goes to Philipp Jenke, who had an enormous influence on the development of my programming skills.

Also I would like to thank Peter Schiansky and Teodor Strömberg who both supplied me with their stock of PCB motors to perform the countless waveplate rotation required for the quantum SWITCH experiment and more importantly for sharing their laser with me. The use of this laser solved in a way the last problem that prevented the success of the experiment.

Of course, I want to thank Philip Walther, who is the main reason our entire group can do this interesting research and for that I believe he is a great leader of the group. Working in his group definitely shaped my future career as a physicist.

Not to forget is Thorsten Schumm, who guided my project from the side of

Die approbierte gedruckte Originalversion dieser Diplomarbeit ist an der TU Wien Bibliothek verfügbar
The approved original version of this thesis is available in print at TU Wien Bibliothek.
TU Bibliothek Your knowledge hub WIEN

the Technical University of Vienna. He made it possible for me to follow my interest and carry out my master thesis on another university, the University of Vienna, and therefore I want to express my deepest thankfulness to him.

Finally, a big thank you goes to the whole group for creating such a great working atmosphere and for the very joyful after-work activities together.

Die approbierte gedruckte Originalversion dieser Diplomarbeit ist an der TU Wien Bibliothek verfügbar
The approved original version of this thesis is available in print at TU Wien Bibliothek.
TU WIEN Bibliothek Your knowledge hub

List of Figures

2.1 Illustration of the feed-forward protocol. 3
2.2 Schematic illustration of the Maxwell's demon thought experiment. 9
2.3 Schematic illustration of a photonic Maxwell's demon with correlated baths. 11
2.4 Visualization of the 2-SWITCH operation. 22
2.5 Illustration of a 'causal witness' and the process matrix. . . . 29

3.1 Experimental setup of the Maxwell's demon experiment. . . . 33
3.2 Experimental setup of the fiber-based quantum SWITCH. . . 36
3.3 Illustration of the time-bin propagation in the quantum SWITCH. 38

4.1 Photon source characterization for the Maxwell's demon experiment. 42
4.2 Measurement results of the 'power' of Maxwell's demon with different input states. 45
4.3 Experimentally estimated probabilities with which two Pauli-operators either commute or anti-commute. 47
4.4 Experimental results of the causal tomography for the case, that Alice and Bob have only access to unitary operations. . . 49
4.5 Experimental results of the causal tomography for the case, that Alice and Bob have both access to measurement/re-preparation channels. 51
4.6 Graphical illustration of the experimentally estimated process matrix of the quantum SWITCH. 53

Die approbierte gedruckte Originalversion dieser Diplomarbeit ist an der TU Wien Bibliothek verfügbar
The approved original version of this thesis is available in print at TU Wien Bibliothek.
TU Bibliothek Your knowledge hub WIEN

Die approbierte gedruckte Originalversion dieser Diplomarbeit ist an der TU Wien Bibliothek verfügbar
The approved original version of this thesis is available in print at TU Wien Bibliothek.

References

[1] G. L. Zanin, M. J. Jacquet, M. Spagnolo, P. Schiansky, I. A. Calafell, L. A. Rozema, P. Walther, "Fiber-compatible photonic feed-forward with 99% fidelity," *Optics Express*, 2021.

[2] J. C. Maxwell, *Theory of Heat.* Longman, 1871.

[3] O. Oreshkov, F. Costa, and Č. Brukner, "Quantum correlations with no causal order," *Nature Communications*, vol. 3, no. 1, p. 1092, 2012.

[4] L. M. Procopio, A. Moqanaki, M. Araújo, F. Costa, I. Alonso Calafell, E. G. Dowd, D. R. Hamel, L. A. Rozema, Č. Brukner, and P. Walther, "Experimental superposition of orders of quantum gates," *Nature Communications*, vol. 6, no. 1, p. 7913, 2015.

[5] G. Rubino, L. A. Rozema, A. Feix, M. Araújo, J. M. Zeuner, L. M. Procopio, Č. Brukne, P. Walther, "Experimental verification of an indefinite causal order," *Science Advances*, vol. 3, no. 3, 2017.

[6] R. Landauer, "Irreversibility and heat generation in the computing process," *IBM Journal of Research and Development*, vol. 5, no. 3, pp. 183–191, 1961.

[7] M. D. Vidrighin, O. Dahlsten, M. Barbieri, M. S. Kim, V. Vedral, and I. A. Walmsley, "Photonic maxwell's demon," *Phys. Rev. Lett.*, vol. 116, p. 050401, Feb 2016.

[8] A. Shu, J. Dai, and V. Scarani, "Power of an optical maxwell's demon in the presence of photon-number correlations," *Phys. Rev. A*, vol. 95, p. 022123, Feb 2017.

[9] G. Chiribella, G. M. D'Ariano, P. Perinotti, and B. Valiron, "Quantum computations without definite causal structure," *Phys. Rev. A*, vol. 88, p. 022318, Aug 2013.

[10] R. Prevedel, P. Walther, F. Tiefenbacher, P. Böhi, R. Kaltenbaek, T. Jennewein, A. Zeilinger, "High-speed linear optics quantum computing using active feed-forward," *nature*, 2007.

Die approbierte gedruckte Originalversion dieser Diplomarbeit ist an der TU Wien Bibliothek verfügbar
The approved original version of this thesis is available in print at TU Wien Bibliothek.
TU Bibliothek Your knowledge hub WIEN

[11] T. Kim, M. Fiorentino, F. N. C. Wong, "Phase-stable source of polarization-entangled photons using a polarization Sagnac interferometer," *Physical Review A*, 2006.

[12] C. C. Gerry and P. Knight, *Introductory quantum optics*, 3rd ed. Cambridge [u.a.]: Cambridge Univ. Press, 2008.

[13] C. H. Bennett, "The thermodynamics of computation—a review," *International Journal of Theoretical Physics*, vol. 21, no. 12, pp. 905–940, 1982.

[14] J. V. Koski, V. F. Maisi, T. Sagawa, and J. P. Pekola, "Experimental observation of the role of mutual information in the nonequilibrium dynamics of a maxwell demon," *Phys. Rev. Lett.*, vol. 113, p. 030601, Jul 2014.

[15] A. Bérut, A. Arakelyan, A. Petrosyan, S. Ciliberto, R. Dillenschneider, and E. Lutz, "Experimental verification of landauer's principle linking information and thermodynamics," *Nature*, vol. 483, no. 7388, pp. 187–189, 2012.

[16] Guilherme L. Zanin and Michael Antesberger and Maxime J. Jacquet and Paulo H. Souto Ribeiro and Lee A. Rozema and Philip Walther, "Enhanced Photonic Maxwell's Demon with Correlated Baths," *arXiv*, 2021.

[17] R. Loudon, *The quantum theory of light*, 3rd ed., ser. Oxford science publications. Oxford: Oxford Univ. Press, 2000.

[18] M. J. Holland and K. Burnett, "Interferometric detection of optical phase shifts at the heisenberg limit," *Phys. Rev. Lett.*, vol. 71, pp. 1355–1358, Aug 1993.

[19] T. Kuusela, "Measurement of the second-order coherence of pseudothermal light," *American Journal of Physics*, vol. 85, pp. 289–294, 04 2017.

[20] W. Martienssen and E. Spiller, "Coherence and fluctuations in light beams," *American Journal of Physics*, vol. 32, no. 12, pp. 919–926, 1964.

[21] B. E. A. Saleh, M. C. Teich, *Fundamentals of Photonics*. Wiley, 2007.

[22] G. Grynberg, A. Aspect, C. Fabre, *Introduction to Quantum Optics*. Cambridge University Press, 2010.

Die approbierte gedruckte Originalversion dieser Diplomarbeit ist an der TU Wien Bibliothek verfügbar
The approved original version of this thesis is available in print at TU Wien Bibliothek.
TU Bibliothek Your knowledge hub WIEN

[23] L. A. Rozema, J. D. Bateman, D. H. Mahler, R. Okamoto, A. Feizpour, A. Hayat, and A. M. Steinberg, "Scalable spatial superresolution using entangled photons," *Phys. Rev. Lett.*, vol. 112, p. 223602, Jun 2014.

[24] M. A. Nielsen and I. L. Chuang, *Quantum computation and quantum information*, 10th ed. Cambridge [u.a.]: Cambridge Univ. Press, 2010.

[25] T. Colnaghi, G. D'Ariano, S. Facchini, and P. Perinotti, "Quantum computation with programmable connections between gates," *Physics Letters A*, vol. 376, pp. 2940–2943, 10 2012.

[26] M. J. Renner and Č. Brukner, "Reassessing the computational advantage of quantum-controlled ordering of gates," *arXiv*, 2021.

[27] P. C. Humphreys, B. J. Metcalf, J. B. Spring, M. Moore, X.-M. Jin, M. Barbieri, W. S. Kolthammer, and I. A. Walmsley, "Linear optical quantum computing in a single spatial mode," *Phys. Rev. Lett.*, vol. 111, p. 150501, Oct 2013.

[28] R. Simon and N. Mukunda, "Minimal three-component su(2) gadget for polarization optics," *Physics Letters A*, vol. 143, no. 4, pp. 165–169, 1990.

[29] O. Gühne and G. Tóth, "Entanglement detection," *Physics Reports*, vol. 474, no. 1, pp. 1–75, 2009.

[30] A. Royer, "Wigner function in liouville space: A canonical formalism," *Phys. Rev. A*, vol. 43, pp. 44–56, Jan 1991.

[31] M. Araújo, C. Branciard, F. Costa, A. Feix, C. Giarmatzi, and Č. Brukner, "Witnessing causal nonseparability," *New Journal of Physics*, vol. 17, 06 2015.

[32] R. H. BROWN and R. Q. TWISS, "Correlation between photons in two coherent beams of light," *Nature*, vol. 177, no. 4497, pp. 27–29, 1956.

[33] B. Blauensteiner, I. Herbauts, S. Bettelli, A. Poppe, and H. Hübel, "Photon bunching in parametric down-conversion with continuous-wave excitation," *Phys. Rev. A*, vol. 79, p. 063846, Jun 2009.

Die approbierte gedruckte Originalversion dieser Diplomarbeit ist an der TU Wien Bibliothek verfügbar
The approved original version of this thesis is available in print at TU Wien Bibliothek.
TU Bibliothek Your knowledge hub WIEN